

Spectral Analysis of the Growth of Translational Superfluid Flow in a Bose Liquid

Shun-ichiro Koh

*Physics Division, Faculty of Education, Kochi University, Akebono-cho, 2-5-1, Kochi, 780, Japan.**

(Dated: October 7, 2021)

Spectral analysis of the translational superfluid flow of a Bose liquid is attempted. When cooling a dissipative flow of liquid helium 4 through a capillary at $T > T_\lambda$, a superfluid flow abruptly appears at T_λ . By a thought experiment in which the pressure difference between two ends of a capillary slowly oscillates, the spectrum of fluidity (the reciprocal of kinematic viscosity) just above T_λ ($2.17\text{K} < T < 2.18\text{K}$) is examined using a sum rule that incorporates the result of linear response theory and fluid mechanics. According to Feynman's picture on the many-body wave function of bosons, as the condensate grows in the flow, the transverse motion in the flow becomes suppressed by the emergence of a gap, originating from the Bose statistics, in the excitation spectrum. This statistical gap induces a continuous change in the fluidity spectrum just above T_λ , which demonstrates the growth of a superfluid flow. For this mechanism, the size distribution of the coherent wave function plays an important role. As a byproduct, a new interpretation of the critical velocity is proposed.

PACS numbers: 67.40.-w

I. INTRODUCTION

Superfluidity has been a mysterious phenomenon since the discovery of a superfluid flow in liquid helium 4 in 1938 [1] [2] [3]. It is classified into a translational superfluid flow and rotational superfluid flow. When the temperature is decreased to T_λ , the former appears in the flow which is until then dissipative at $T > T_\lambda$ as in a flow in a capillary, and the latter appears in the flow which is until then nondissipative (in principle) at $T > T_\lambda$ as in a flow in a rotating bucket. In comparison with the rotational superfluid flow, questions still remain to be answered in the translational superfluid flow, because it is more directly concerned with the irreversible processes in liquids [4]. When cooling liquid helium 4 flowing in a capillary, the coefficient of kinematic viscosity $\nu(T)$ gradually decreases in the range of $T_\lambda < T < 3.7$ K, finally reaching zero at T_λ , as shown in Fig. 1 [5][6][7]. In the range of 2.17 K $< T < 2.18$ K, superfluid flow abruptly grows within a narrow temperature region of less than 0.01 K. Behind this seemingly abrupt decrease in viscosity, we can see a remarkable phenomenon: When the external parameter falls below the critical value, the complex process transforms to a simple one by the formation of order (the inverse of bifurcation [8]). In this paper, we derive $\rho_s \mathbf{v}_s$ in the two-fluid mechanics from the normal flow just above T_λ , and consider the transition of a laminar viscous flow to a translational superfluid flow of a Bose liquid from viewpoint of spectrum analysis.

(a) In the normal phase, the flow in a capillary is described as Poiseuille's flow in fluid mechanics. When a pressure difference P between two ends of a capillary (circular cross section with radius d , and length L) is applied to a normal liquid with density ρ and coefficient of shear

viscosity η , the Navier–Stokes equation with Stokes's approximation,

$$\rho \frac{\partial \mathbf{v}}{\partial t} = \eta \nabla^2 \mathbf{v} - \nabla P, \quad (1)$$

gives the fluid velocity of a steady flow as a function of radial distance r from the axis of capillary as follows:

$$\mathbf{v}(r) = \frac{d^2 - r^2}{4\eta} \frac{\mathbf{P}}{L}. \quad (2)$$

This formula is a dissipative-type relation $v \propto P$, similar to a terminal velocity which a raindrop falling from the atmosphere reaches before falling to the ground. Let us view this system on a reference frame moving with velocity \mathbf{v} . To study the change from a normal flow to a superfluid flow, we consider the longitudinal motion and the transverse motion in normal flow, and decompose them into excitations with different momenta and frequencies. The infinite-wavelength limit ($q \rightarrow 0$) of the longitudinal excitation is equivalent to the uniform translation of a liquid. Hence, at this limit, excitations with small momenta and frequencies are smoothly transformed to a translational superfluid flow. The growth of a superfluid flow is a process in which other excitations with finite q , contained in the viscous flow at $T > T_\lambda$, converge to the superfluid flow with $q = 0$. Although the superfluid flow is a steady flow, the spectrum analysis of the viscous flow near T_λ gives us important information on the growth of superfluid flow.

Along this line, we consider a thought experiment in which a slowly oscillating pressure difference is applied to a fluid as $P(\omega) \exp(-i\omega t)$, which is an extension of the oscillatory Poiseuille's flow experiment [9]. In the case of a normal liquid, an oscillating mass-flux density $\mathbf{j}(\omega) = \rho \mathbf{v}(\omega)$ appears along the axis of the capillary in Eq.(2) [10],

$$\mathbf{j}(\omega) = \sigma(\omega) d^2 \frac{\mathbf{P}(\omega)}{L}, \quad (3)$$

*Electronic address: koh@kochi-u.ac.jp

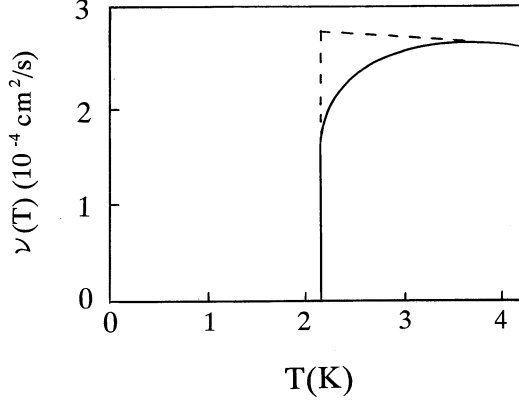


FIG. 1: The coefficient of kinematic viscosity $\nu(T)$ (solid curve) of the capillary flow of liquid helium 4. [The dashed line illustrates $\nu(T)$ when the gradual decrease in $\nu(T)$ does not occur.]

where $\sigma(\omega) = \rho/(4\eta) = 1/(4\nu)$ is the frequency spectrum of fluidity, the dimension of which is $(length)^{-2}(second)$. [From now, we simply call $j(\omega)$ a flow, and call $\sigma(\omega)$ a *fluidity spectrum* of a liquid.] This $\sigma(\omega)$ of the normal liquid is calculated in fluid mechanics as follows. Under the oscillating pressure gradient $P(\omega) \exp(-i\omega t)/L$, Eq.(1) is written in cylindrical polar coordinate as

$$\frac{\partial v}{\partial t} = \nu \left(\frac{\partial}{\partial r^2} + \frac{\partial}{r\partial r} \right) v + \frac{P(\omega) \exp(-i\omega t)}{\rho L}, \quad (4)$$

where $\nu = \eta/\rho$. The velocity $v(r, t)$ at a distance r from the axis has the form

$$v(r, t) = \frac{P(\omega) \exp(-i\omega t)}{-i\omega\rho L} + \delta v(r, t), \quad (5)$$

where $\delta v(r, t)$ satisfies

$$\frac{\partial \delta v(r, t)}{\partial t} = \nu \left(\frac{\partial}{\partial r^2} + \frac{\partial}{r\partial r} \right) \delta v(r, t). \quad (6)$$

The solution $\delta v(r, t)$ of Eq.(6) is written in terms of the Bessel function as $J_0(i\lambda_0 r) \exp(-i\omega t)$ with $\lambda_0 = (1-i)\sqrt{\omega/(2\nu)}$ [11]. Using this $J_0(i\lambda_0 r) \exp(-i\omega t)$ as $\delta v(r, t)$, and setting $v(d, t) = 0$ in Eq.(5) as a boundary condition, we obtain

$$v(r, t) = \frac{P(\omega) \exp(-i\omega t)}{-i\omega\rho L} \left(1 - \frac{J_0(i\lambda_0 r)}{J_0(i\lambda_0 d)} \right). \quad (7)$$

With this $v(r, t)$ at $r = 0$ used in $\rho v(0, t) = \sigma(\omega) d^2 P(\omega) \exp(-i\omega t)/L$ of Eq.(3), the fluidity spectrum $\sigma(\omega)$ in the oscillatory Poiseuille's flow is given by

$$\sigma(\omega) = \frac{-1}{\omega d^2} \text{Im} \left(1 - \frac{1}{J_0 \left(id[1-i]\sqrt{\frac{\rho}{2\eta}\omega} \right)} \right), \quad (8)$$

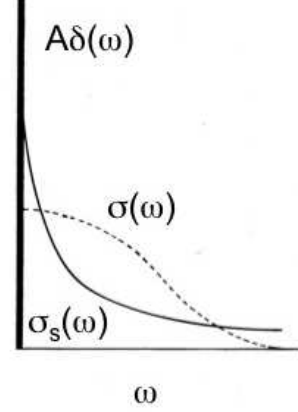


FIG. 2: Schematic view of the fluidity spectrum $\sigma_s(\omega) + A\delta(\omega)$ characterizing a superfluid flow. The dotted curve represents $\sigma(\omega)$ for a normal liquid in Eq.(8). $\sigma(0)$ is inversely proportional to ν in Fig.1.

which is schematically shown as a dotted curve in Fig.2. The fluidity of a flow through a capillary gradually falls with the increase in frequency of the pressure oscillation. Expanded in powers of ω , $\sigma(\omega)$ in Eq.(8) has the following form

$$\sigma(\omega) = \frac{\rho}{4\eta_n} \left[1 - \frac{d^4}{576} \left(\frac{\omega}{\eta_n/\rho} \right)^2 + \dots \right]. \quad (9)$$

This $\sigma(\omega)$ does not substantially fall near $\omega = 0$ [in this case, $\eta_n/(\rho d^2) \simeq 2 \times 10^{-2}$ [1/s]], implying that the viscous flow is robust when the applied pressure slowly oscillates. In this paper, we address a question of how the growth of a superfluid flow changes this feature.

(b) In the superfluid phase, owing to the growth of a condensate, the $\rho v \propto P$ -type relation in Eq.(3) changes to a nondissipative Newtonian law $\rho a \propto P$, where a is acceleration. This change implies that once pressure is applied to this liquid at the beginning, a nonzero flow ($j \neq 0$) continues to exist even after the pressure difference is removed ($P = 0$). Such a phenomenon can be described by Eq.(3) only when $\sigma(\omega)$ shows divergence at $\omega = 0$. [The abrupt increase in σ implies the vertical fall of $\nu = 1/(4\sigma)$ as in Fig.1.] This divergence at $\omega = 0$ is not an isolated phenomenon in the frequency. Since the values of $\sigma(\omega)$ at finite ω and at $\omega = 0$ represent the same growth process at different frequencies, the most probable form of the fluidity spectrum in a superfluid flow is illustrated in Fig.2, which is given by

$$j(\omega) = [\sigma_s(\omega) + A(T)\delta(\omega)] d^2 \frac{P(\omega)}{L}, \quad (10)$$

where $A(T)$ is a constant to be determined. $\sigma_s(\omega)$ includes information on the precursory form of a superfluid flow of mesoscopic size. An interesting point is

whether this $A(T)$ is different from the thermodynamic rate $\rho_s(T)/\rho$. This $\sigma_s(\omega) + A(T)\delta(\omega)$ is a sign of a translational superfluid flow emerging in the dissipative process. As an early study along this line, we studied the frequency-expansion of $\sigma_s(\omega) + A(T)\delta(\omega)$ in the vicinity of T_λ [12]. In the present paper, by considering the effect of Bose statistics on the flowing coherent many-body wave function more concretely, we will derive a precise form of the fluidity spectrum in all frequencies, and incorporate it into a sum rule.

To study the change from Eq.(3) to Eq.(10), it is useful to focus on a relation holding both at $T > T_\lambda$ and $T \leq T_\lambda$. The fluidity spectrum must satisfy a sum rule. To illustrate its physical meaning, let us consider the following equation of motion under pressure with a relaxation time τ :

$$m \frac{dv}{dt} = Pd^2 - \frac{m}{\tau}v. \quad (11)$$

Under the oscillating pressure $P \exp(-i\omega t)$, the oscillating velocity is given by

$$v(\omega) = \frac{Pd^2}{m} \left(\frac{\tau^{-1}}{\omega^2 + \tau^{-2}} + i \frac{\omega}{\omega^2 + \tau^{-2}} \right). \quad (12)$$

Comparing it to $j(\omega) = \rho v(\omega) = \sigma(\omega)d^2P/L$, we obtain

$$\sigma(\omega) = \frac{\rho L}{m} \left(\frac{\tau^{-1}}{\omega^2 + \tau^{-2}} + i \frac{\omega}{\omega^2 + \tau^{-2}} \right). \quad (13)$$

Hence, we obtain the sum rule

$$\int_{-\infty}^{\infty} \text{Re}\sigma(\omega)d\omega = \pi \frac{\rho L}{m}. \quad (14)$$

In this derivation, τ is necessary, but it disappears in the final result. The right-hand side of Eq.(14) includes only parameters in setting experiments, which is a feature of general relations (see Appendix A). Hence, the change in the fluidity spectrum $\sigma(\omega)$ from Eq.(3) to Eq.(10) around T_λ must satisfy

$$\int_{-\infty}^{\infty} \sigma(\omega)d\omega = \int_{-\infty}^{\infty} [\sigma_s(\omega) + A(T)\delta(\omega)]d\omega. \quad (15)$$

Substituting the concrete formula of the fluidity spectrum into both sides, we can examine how the superfluid flow grows out of the viscous flow.

(c) Behind the above change in $\sigma(\omega)$, some physical process must exist. A superfluid flow withstands thermal dissipation, which implies that there must be a gap in the excitation-energy spectrum. (Do not confuse this gap with the roton gap in the phonon spectrum of liquid helium 4.) In two-fluid mechanics, Landau assumed the irrotationality constraint $\text{rot}v_s = 0$ on the superfluid velocity, which implies that the low-energy excitation of a transverse nature is suppressed in a superfluid. Hence, such a gap must exist in the spectrum of transverse excitation. In this respect, a suggestive consideration was

given by Feynman in the 1950s [13]. Despite the dissipation of energy in liquids, the longitudinal spectrum (that is, acoustic phonon) was clearly observed by the inelastic neutron diffraction in the superfluid phase of liquid helium 4. The central problem is explaining why no states other than the acoustic phonon can have low energies. Feynman considered that an energy gap owing to Bose statistics clearly separates the spectrum of the acoustic phonon from that of other excitations. Consider a free particle inside a box of size L_0 . The lowest eigenvalue of the Laplacian is of the order of $\sim 1/L_0^2$. This is realized by an excitation with the longest possible wavelength $\lambda \sim L_0$. When λ is finite, the spectrum $\epsilon(q)$ of such a system has a gap at $q = 0$. Consider the displacement of particles in the condensate. When the permutation symmetry of Bose statistics holds, multiple permutation, operated on the distribution of particles after displacement, results in a final distribution which is apart from the initial displacement only by a small distance similar to the interatomic distance r_0 in liquid. Hence, a large L_0 is not possible, and such a L_0 is reduced to the interatomic distance r_0 in a liquid. The kinetic energy, determined by the square of the spatial derivative of the wave function ψ , cannot have an excitation energy lower than a limit as follows:

$$\frac{\hbar^2}{2m}(\nabla\psi)^2 \geq \frac{\hbar^2}{2m} \frac{(\delta\psi)^2}{r_0^2}. \quad (16)$$

In liquid helium 4, where the interatomic distance is $r_0 \simeq 5 \times 10^{-11}$ [m] and the mass of a helium 4 atom is $m = 6.7 \times 10^{-27}$ [kg] [14], we obtain $\epsilon_0 \equiv (\hbar^2/2m)(1/r_0^2) \simeq 3.0 \times 10^{-22}$ [J]. This ϵ_0 is much larger than $\hbar\omega$ realized in the hydrodynamic experiments, and therefore this ϵ_0 completely suppresses such a transverse excitation in a Bose liquid. Since this gap is due to Bose statistics, not to the particle interaction, we will call this ϵ_0 a statistical gap.

This explanation is also applicable to the nonequilibrium steady process. The problem is whether such a permutation is possible on a macroscopic scale in the flow. In the Bose system, permutation is always possible locally between adjacent particles. However, whether macroscopic permutation between distant particles is possible depends on the type of flow pattern. Only when the displacement vectors are transverse with respect to the flow direction, permutation on the macroscopic scale is possible. Hence, the point to be considered is whether the transverse excitation occurs within or beyond the coherent wave function. Near T_λ , various sizes of coherent wave functions appear in the Bose liquid. Using their size distribution in this paper, we will clarify the mechanism by which the statistical gap in the transverse motion changes the fluidity spectrum from $\sigma(\omega)$ to $\sigma_s(\omega) + A(T)\delta(\omega)$, and explain the growth process of a superfluid flow in the range of $2.17 \text{ K} < T < 2.18 \text{ K}$.

Phenomena near T_λ are affected by fluctuation. However, for the fluctuation in nonequilibrium steady states, an example of which is a flowing liquid near T_λ , a con-

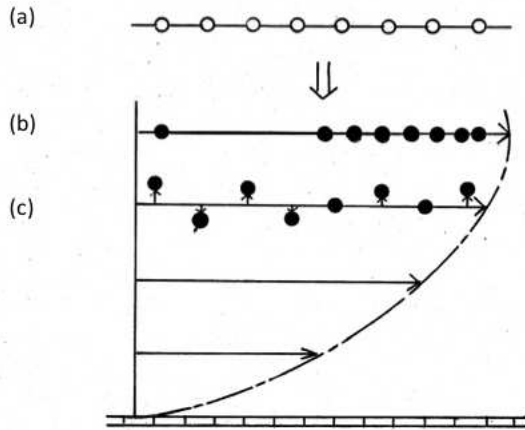


FIG. 3: Schematic view of the microscopic relative displacement of particles in a normal capillary flow when one views them on a moving frame: (b) longitudinal and (c) transverse displacements from (a) the initial uniform distribution. The real image is a mixture of these two types of displacements, the lengths of which are exaggerated for clarity. The macroscopic one-directional velocity $\mathbf{v}(r)$ of Poiseuille's flow [Eq.(2)] is illustrated for reference.

vincing theoretical description has yet to be found [15]. Hence, we ignore such a fluctuation in this paper, and regard results obtained in this paper as a first step to the complete statistical theory.

This paper is organized as follows. In Sec.2, we explain the nature of the statistical gap appearing in the transverse motion in the flow, and introduce the size distribution of the coherent many-body wave function. In Sec.3, we formulate Poiseuille's flow by rewriting Eq.(3) as a linear-response relation, then formulating the two-fluid model in terms of the fluidity spectrum. In Sec.4, we derive the change in the fluidity spectrum from $\sigma(\omega)$ to $\sigma_s(\omega) + A\delta(\omega)$ in Fig.2 by combining the linear response theory and fluid mechanics in the sum rule. In Sec.5, we perform a model calculation using the result of Sec.4. In view of the concrete form of $\sigma_s(\omega)$ in Sec.5.D, a new interpretation of the critical velocity of a superfluid flow is proposed. In Sec.6, we discuss remaining problems.

II. PHYSICAL VIEW OF TRANSLATIONAL SUPERFLUID FLOW

A. Longitudinal motion and transverse motion in the flow

(a) Figure 3 schematically illustrates particles in a normal liquid flowing through a capillary. When one views them on a moving frame from left to right, one notes

two types of microscopic relative displacements of particles. Let us imagine a relative position $(\mathbf{x}_1, \dots, \mathbf{x}_s)$ of s particles on a streamline, which changes to $[\mathbf{x}_1 + \delta\mathbf{R}(\mathbf{x}_1), \dots, \mathbf{x}_s + \delta\mathbf{R}(\mathbf{x}_s)]$. We can classify the relative displacements $\delta\mathbf{R}(\mathbf{x}_i)$ into longitudinal $\delta\mathbf{R}^l$ and transverse $\delta\mathbf{R}^t$ displacements such that $\delta\mathbf{R}^l \parallel \mathbf{q}$ and $\delta\mathbf{R}^t \perp \mathbf{q}$, where \mathbf{q} is along the flow direction. In Fig.3, particles make longitudinal displacements (b) from the initial uniform distribution (a). Similarly, particles make transverse displacements (c), which is the origin of shear viscosity by transferring the momentum from one streamline to another. In reality, the relative displacement in the flow is a mixture of these two types of displacements $\delta\mathbf{R} = \delta\mathbf{R}^l + \delta\mathbf{R}^t$.

An important difference between these two types of displacements is as follows.

(1) Each vector $\delta\mathbf{R}^l$ of the longitudinal displacement is parallel to the flow, and therefore $\delta\mathbf{R}^l(\mathbf{x}_i)$ of i -th particle in $(\mathbf{x}_1, \dots, \mathbf{x}_s)$ is added to $\delta\mathbf{R}^l(\mathbf{x}_{i+1})$ of the neighboring particles on the streamline as in Fig.3(b). Many $\delta\mathbf{R}^l(\mathbf{x}_i)$ are accumulated in the final distribution $\delta\mathbf{R}_{n+1}^l = \sum_{i=1}^n \delta\mathbf{R}_i^l$. As a result, the longitudinal displacements induce an extensive change in the particle distribution, and therefore, after the longitudinal displacement, nearby particles do not always exist in the initial distribution. Hence, $(\mathbf{x}_1 + \delta\mathbf{R}^l(\mathbf{x}_1), \dots, \mathbf{x}_s + \delta\mathbf{R}^l(\mathbf{x}_s)) \equiv (\mathbf{x}'_1, \dots, \mathbf{x}'_s)$ cannot be reproduced by permutation of the initial $(\mathbf{x}_1, \dots, \mathbf{x}_s)$, which means that the distance between $(\mathbf{x}'_1, \dots, \mathbf{x}'_s)$ and $(\mathbf{x}_1, \dots, \mathbf{x}_s)$ can be large in the configuration space.

(2) In contrast, $\delta\mathbf{R}^t$ of the transverse displacement is perpendicular to the flow, and therefore $\delta\mathbf{R}^t(\mathbf{x}_i)$ of each particle is not additive as in Fig.3(c). Such transverse $\delta\mathbf{R}^t$ are not accumulated, thus no extensive change in the particle distribution is induced. For any given particle after displacement, a nearby particle always exists in the initial distribution. Only by permutation of such particles, can the original distribution be reproduced. In Bose statistics, owing to permutation symmetry, one cannot distinguish the following two types of particles after displacement: one moved from a near position by a short displacement vector, and the other moved from a distant position by a long displacement vector. As long as such transverse displacements occur within the coherent wave function, we cannot distinguish the long and short displacements. The distance between the initial and final distributions in configuration space is, after multiple permutations, finally reduced to a small distance having the order of the interatomic distance r_0 in the liquid. For a given point $(\mathbf{x}_1, \dots, \mathbf{x}_s)$ in configuration space, the region that transverse $(\mathbf{x}_1 + \delta\mathbf{R}^t(\mathbf{x}_1), \dots, \mathbf{x}_s + \delta\mathbf{R}^t(\mathbf{x}_s))$ occupies is located much closer to this point than in the case of longitudinal displacements. As \mathbf{q} in $\chi_{\mu\nu}(\mathbf{q}, \omega)$ approaches zero in a boson's flow, this difference between the longitudinal and transverse displacements becomes more evident.

(b) Let us consider the kinetic energy of such a system.

Since the translational motion is possible only in the z -direction in a capillary, we define a collective coordinate of the translation as

$$\xi_z = \frac{1}{s} \sum_{n=1}^s z_n. \quad (17)$$

The corresponding momentum π_z is determined so that it satisfies a commutation relation $[\pi_z, \xi_z] = -i\hbar$ as

$$\pi_z = -i\hbar \sum_{n=1}^s \frac{\partial}{\partial z_n}. \quad (18)$$

From the kinetic energy of the many-body system

$$T = \frac{\hbar^2}{2m} \sum_{n=1}^s \left(\frac{\partial^2}{\partial x_n^2} + \frac{\partial^2}{\partial y_n^2} + \frac{\partial^2}{\partial z_n^2} \right) \psi(\mathbf{x}_1, \dots, \mathbf{x}_s), \quad (19)$$

we can extract the kinetic energy of the translational motion as a collective mode [16], with the result that

$$\begin{aligned} T &= \frac{\hbar^2}{2M} \left(\sum_{n=1}^s \frac{\partial}{\partial z_n} \psi(\mathbf{x}_1, \dots, \mathbf{x}_s) \right)^2 \\ &+ \frac{\hbar^2}{2m_{ef}} \sum_{n=1}^s \frac{\partial^2}{\partial z_n^2} \psi(\mathbf{x}_1, \dots, \mathbf{x}_s) \\ &+ \frac{\hbar^2}{2m} \sum_{n=1}^s \left(\frac{\partial^2}{\partial x_n^2} + \frac{\partial^2}{\partial y_n^2} \right) \psi(\mathbf{x}_1, \dots, \mathbf{x}_s). \quad (20) \end{aligned}$$

The first term is the kinetic energy of the translational motion responsible for $A(T)\delta(\omega)$ in the fluidity [Eq.(15)], and the second and third terms are those of the internal motion responsible for $\sigma_s(\omega)$. ($M = sm$ is the total mass of s particles, and m_{ef} is the effective mass of the internal motion along the z -direction.)

In general, the excited-state wave function $\psi(\mathbf{x}_1, \dots, \mathbf{x}_s)$ is orthogonal to the ground-state one $\psi_0(\mathbf{x}_1, \dots, \mathbf{x}_s)$. Since the latter has a constant amplitude, the former must spatially oscillate between the positive and negative values. Since the distance between the longitudinal displacement $(\mathbf{x}_1^l, \dots, \mathbf{x}_s^l)$ and the initial one $(\mathbf{x}_1, \dots, \mathbf{x}_s)$ along the z -direction can be large, the derivatives of the wave function $\partial\psi/\partial z_i$ or $\partial^2\psi/\partial z_i^2$ do not have a large value. The kinetic energy of the longitudinal motion [first and second terms in Eq.(20)] can have an infinitely small value, and a gap does not appear in its excitation spectrum.

On the other hand, since a large transverse displacement is not possible owing to permutation symmetry, the distance between the transverse displacement $(\mathbf{x}_1^t, \dots, \mathbf{x}_s^t)$ and the initial one $(\mathbf{x}_1, \dots, \mathbf{x}_s)$ is not large. Hence, the derivatives of the wave function $\partial^2\psi/\partial x_i^2$ or $\partial^2\psi/\partial y_i^2$ do not have a small value. Owing to a steep increase and decrease in amplitude within a short distance, the kinetic energy of the internal motion [third term in Eq.(20)] increases the transverse excitation energy [13]. As a result, the transverse motion within the

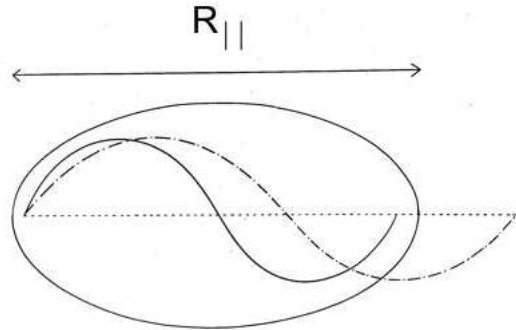


FIG. 4: Average form of the coherent many-body wave function shown as an ellipsoid with major axis R_{\parallel} along the flow. The solid curve represents the transverse displacement from the horizontal dotted straight line within the coherent wave function, and the one-point-dotted curve represents that beyond the coherent wave function. For a given ω , the critical size s_1 of the coherent wave function for distinguishing the above two cases is given by Eq.(50).

coherent wave function is suppressed by this statistical gap having the order of $\epsilon_0 = (\hbar^2/2m_t)(1/r_0^2) = \hbar a_t/r_0^2$ as in Eq.(16), which explains the rigidity of the coherent wave function. To put it simply, the kinetic energy of the superfluid flow is composed only of the first and second terms in Eq.(20) [17].

In summary, during the growth of a superfluid flow, permutation symmetry by Bose statistics plays a role similar to the long-range interaction, while the repulsive short-range interaction U determines the interatomic distance r_0 . Both interactions cooperate to realize the macroscopic superfluid flow.

(c) The statistical gap changes the shear viscosity as follows. In the fluctuation-dissipation theorem, the shear viscosity coefficient η [18] of a flowing liquid along the z -axis is represented by

$$\eta = \frac{1}{k_B T V} \int_0^{\infty} \langle S^{rz}(t) S^{rz}(0) \rangle dt, \quad (21)$$

where S^{rz} stands for the stress tensor

$$S^{rz}(t) = \sum_i^N \frac{1}{m} (p_i^x + p_i^y) p_i^z + \frac{1}{2} \sum_i^N \sum_j^N r_{ij} \frac{\partial U}{\partial z_{ij}}, \quad (22)$$

where the second term is the effect of the repulsive interaction. The transverse motion along the direction perpendicular to the flow in the condensate is suppressed by the statistical gap, and the resulting zero transverse momenta p_i^x and p_i^y of each particle cause the shear viscosity η to vanish. The fluidity of a superfluid flow with such $\eta = 0$ is given by $A(T)\delta(\omega)$ in Eq.(10).

(d) For $\sigma_s(\omega)$ in Eq.(10), the statistical gap in the transverse motion strongly affects the spectrum of flu-

idity as follows. The angular frequency ω in $\sigma_1(\omega)$ corresponds to the time scale at which we observe the dynamics of a flow. In this case, the transverse excitation energy $\epsilon_t(s, q)$ depends on whether the wavelength $\lambda = 2\pi/q$ of the excitation exceeds the length R_{\parallel} of the coherent wave function, as illustrated in Fig.4. If the one-particle transverse excitation occurs within the coherent wave function, it is suppressed by the statistical gap as $\epsilon_t(s, q) = \epsilon_0$, but if the excitation occurs beyond this wave function, permutation symmetry does not hold for particles involved in this excitation, and it has an ordinary one-particle transverse-excitation energy $\epsilon_t(s, q) = (\hbar q)^2/2m_t = \hbar a_t q^2$. Hence, to study the growth process of a superfluid flow, we must take into account the size distribution of the coherent many-body wave function in the flow.

B. Size distribution of coherent many-body wave function

In a condensate near T_{λ} , there are large or small coherent wave functions. To estimate the effect of the statistical gap ϵ_0 on the flow, we need the size distribution $h(s)$ of the coherent wave function in the flow. Here, we simply approximate the Hamiltonian as $H = \sum[\epsilon_p + U_0]$, where the constant U_0 is the mean-field value of the repulsive interaction energy per particle. The grand partition function of bosons in local equilibrium $Z_0(\mu) = \prod(1 - e^{-\beta(\epsilon_p + U_0 - \mu)})^{-1}$, where $\mu_0(T)$ is the chemical potential of the ideal boson gas, is rewritten as

$$Z_0(\mu) = \exp \left[- \sum_p \ln(1 - z e^{-\beta \epsilon_p}) \right], \quad (23)$$

where $z = \exp(\beta[\mu_0 - U_0])$. We define a new $\mu(T)$ as $\mu_0(T)$ including U_0

$$\mu(T) = - \left(\frac{g_{3/2}(1) \times 3}{4\sqrt{\pi}} \right)^2 k_B T_{\lambda} \left(\frac{T - T_{\lambda}}{T_{\lambda}} \right)^2 - U_0, \quad (24)$$

where $g_{3/2}(1) = \sum_{n=1}^{\infty} n^{-3/2} = 2.612$ (Appendix.B). With decreasing temperature, the chemical potential $\mu_0(T)$ of the ideal Bose gas approaches zero, but U_0 is a finite quantity in the liquid. By changing U_0 , we can control how many particles participate in the condensate at T_{λ} .

In the grand canonical ensemble, the particle number s appears in the energy as μs . Hence, if we expand $Z_0(\mu)$ in powers of $z = \exp(\beta\mu)$, it yields the size distribution of the coherent wave function. The exponent in Eq.(23) for $p = 0$ and $p \neq 0$ is expanded in powers of z as

$$\ln(1 - z) = - \sum_{s=1}^{\infty} \frac{z^s}{s}, \quad (25)$$

for $p = 0$, and expanded as

$$\frac{4}{\sqrt{\pi}} \int_0^{\infty} x^2 \ln(1 - z e^{-x^2}) dx = - \sum_{s=1}^{\infty} \frac{z^s}{s^{5/2}}, \quad (26)$$

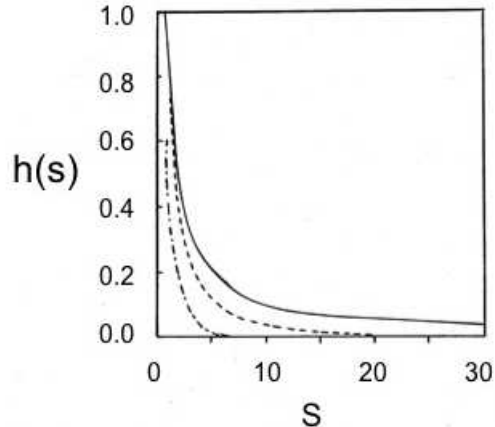


FIG. 5: Size distribution $h(s) = \exp(\beta\mu s)/s$ for $p = 0$ of the coherent many-body wave functions at different temperatures: $h(s)$ at $1.5T_{\lambda}$ (one-point dotted line), at $1.2T_{\lambda}$ (dotted line), and at T_{λ} (solid line).

for $p \neq 0$, where \sum_p in Eq.(23) is transformed to an integral over $x = \sqrt{\beta\epsilon_p}$. With these expansions used in Eq.(23), we obtain the following $Z_0(\mu)$ [19]:

$$Z_0(\mu) = \exp \left[V \sum_{s=1}^{\infty} \left(\frac{e^{\beta\mu s}}{s} + \frac{V}{2\lambda_t^3} \frac{e^{\beta\mu s}}{s^{5/2}} \right) \right], \quad (27)$$

where $\lambda_t = \sqrt{2\pi\hbar^2\beta/m}$ is the thermal wavelength. The equation of states $N = k_B T \partial \ln Z_0 / \partial \mu$ with this $Z_0(\mu)$ is written as a sum over the size s of the coherent many-body wave function

$$\frac{N}{V} = \sum_{s=1}^{\infty} \left(e^{\beta\mu s} + \frac{V}{2\lambda_t^3} \frac{e^{\beta\mu s}}{s^{1.5}} \right). \quad (28)$$

In Eq.(28), each term on the right-hand side represents the number density of particles belonging to the coherent many-body wave function including s particles. (For the combinatorial derivation of Eq.(27), see Appendix C.) Dividing each term in Eq.(28) by s , one obtains the size distribution $h(s)$ of the coherent many-body wave function

$$h(s) = \frac{\exp(\beta\mu s)}{s}, \quad p = 0 \quad (29)$$

$$h(s) = \frac{V}{2\lambda_t^3} \frac{\exp(\beta\mu s)}{s^{2.5}}, \quad p \neq 0 \quad (30)$$

in analogy with the cluster expansion of the equation of states in a classical gas. Figure 5 shows $h(s)$ for $p = 0$. As the temperature approaches T_{λ} , it changes from a

rapidly falling function of s at $1.5T_\lambda$ to a function extending to large s at T_λ . As will be explained in Sec.4, the lower-convex form of $h(s)$ in Fig.5 translates to the lower-convex form of $\sigma_1(\omega)$ of superfluid flow in Fig.2 through the Kramers–Kronig relation. While the left-hand side of Eqs.(25) and (26) is well known as the one-particle distribution of Bose statistics, the right-hand side is useful for the argument regarding the size of the coherent wave function.

Apart from this $h(s)$, we do not have sufficient information on the shape of the coherent wave function in the flowing liquid. However, it is natural to assume that its average shape is a compact form, which is symmetric with respect to the rotation around the direction of flow. A compact form with such a symmetry is the ellipsoid $(x^2 + y^2)/R_\perp^2 + z^2/R_\parallel^2 = 1$, as illustrated in Fig.4, with major axis R_\parallel (parallel to the flow along the z -axis) and minor one R_\perp (on the $x - y$ plane perpendicular to the flow). The number s of particles included in the coherent wave function is proportional to the volume of the ellipsoid as $(4\pi/3)R_\parallel R_\perp^2 = sr_0^3$. The shape of the ellipsoid (the ratio of R_\parallel to R_\perp) depends on s , which is represented by $R_\parallel \simeq s^Z r_0$ and $R_\perp \simeq s^{2X} r_0$ with $Z + 2X = 1$. When the condensate grows in a liquid at rest, its average shape is a sphere with $Z = 1/3$. However, when the coherent wave function appears in a flowing liquid at a low temperature, there is already a velocity distribution $\mathbf{v}(\mathbf{r})$, as shown in Fig.3, and therefore, the coherent wave function, which rides on this $\mathbf{v}(\mathbf{r})$, is elongated along the flow direction (z -axis). The ellipsoid is likely to be more elongated as s increases. In reality, the average shape of the coherent many-body wave function in the flow is likely to have a value of Z near to 1.

In Sec.3, we prepare the linear-response formalism for the fluidity spectrum $\sigma_1(\omega)$, and in Sec.4, we will combine $h(s)$ in Fig.5 with the image in Fig.4 using the formalism prepared in Sec.3.

III. FLUIDITY SPECTRUM AND TRANSLATIONAL SUPERFLUID FLOW.

A. Fluidity spectrum as a linear-response coefficient

Let us consider a repulsive Bose system with the following Hamiltonian

$$H = \sum_p \epsilon(p) \psi_p^\dagger \psi_p + U \sum_{p,p'} \sum_q \psi_{p-q}^\dagger \psi_{p'+q}^\dagger \psi_{p'} \psi_p \quad (U > 0). \quad (31)$$

The fluidity spectrum $\sigma(\omega)$ in Eq.(3) can be generalized from a real to a complex number

$$\mathbf{j}(\omega) = [\sigma_1(\omega) + i\sigma_2(\omega)] d^2 \frac{\mathbf{P}(\omega)}{L}. \quad (32)$$

In contrast to the mechanical perturbation which is directly exerted on particles such as the electric field on

electrons, the pressure difference P between the two ends of a capillary is a thermal perturbation, which is a far more complex phenomenon. Among some formalisms dealing with this problem [20], we will adopt the simplest one called the *indirect method*. To incorporate Eq.(32) into the linear-response theory, we will define, instead of $P(t) = P(\omega) \exp(-i\omega t)$, a fictitious momentum-like field $Q(t) = Q(\omega) \exp(-i\omega t)$ satisfying the following equation of motion [21]

$$\frac{dQ(t)}{dt} = \frac{P(t)}{L}. \quad (33)$$

This $Q(\omega)$ can be regarded as constituting the perturbation energy as

$$\frac{1}{\rho} \int j(\omega) Q(\omega) d\omega. \quad (34)$$

Instead of $P(\omega)$, we can formally regard $Q(\omega)$ as an external field inducing $j(\omega)$ in Eq.(32). Here, we make an approximation that this $Q(\omega)$ is instantaneously exerted on the flow $\mathbf{j}(\omega)$ similarly to the true mechanical one. Since a liquid is a system with high density, the effect of pressure, represented by $Q(\omega)$, rapidly propagates through the liquid in a capillary. Compared with a gas in which such a propagation requires considerable time, this approximation is not an unrealistic one in a liquid, especially for the slow perturbation.

We obtain a bosonic analogue of the London equation in superconductivity by rewriting Eq.(32), using $P(\omega)/L = -i\omega Q(\omega)$ of Eq.(33), as

$$\mathbf{j}(\omega) = [\omega\sigma_2(\omega) - i\omega\sigma_1(\omega)] d^2 \mathbf{Q}(\omega), \quad (35)$$

and regard $[\omega\sigma_2(\omega) - i\omega\sigma_1(\omega)] d^2$ as a spatially averaged form of the generalized susceptibility. In this formula, one can regard the real part $\omega\sigma_2(\omega)$ as representing the nondissipative process, and the imaginary part $-i\omega\sigma_1(\omega)$ as representing the dissipative one.

The fluctuation-dissipation theorem says that the nonequilibrium behavior of the system, which is slightly deviated from the equilibrium state, is described by the generalized susceptibility $\chi_{\mu\nu}(\mathbf{q}, \omega)$ of the equilibrium state. Microscopically, the capillary flow of a superfluid is described by the generalized susceptibility composed of the flow-flow correlation.

$$\chi_{\mu\nu}(\mathbf{q}, i\omega_n) = -\frac{1}{V} \int_0^\beta d\tau \exp(i\omega_n \tau) \langle 0 | T_\tau J_\mu(\mathbf{q}, \tau) J_\nu(\mathbf{q}, 0) | 0 \rangle, \quad (36)$$

where

$$J_\mu(\mathbf{q}, \tau) = \sum_n \sum_p \hbar \left(p + \frac{q}{2} \right)_\mu \psi_p^\dagger \psi_{p+q} \exp(i\omega_n \tau). \quad (37)$$

Behind the macroscopic velocity $v(r)$ in Eq.(2), the microscopic velocity of each particle has not only longitudinal but also transverse components. Accordingly, the

generalized susceptibility consists of the longitudinal and transverse parts ($\mu, \nu = x, y, z$)

$$\chi_{\mu\nu}(\mathbf{q}, \omega) = \chi^L(\mathbf{q}, \omega) \frac{q_\mu q_\nu}{q^2} + \chi^T(\mathbf{q}, \omega) \left(\delta_{\mu\nu} - \frac{q_\mu q_\nu}{q^2} \right). \quad (38)$$

In a rotational superfluid flow, $\chi_{\mu\nu}(\mathbf{q}, \omega)$ describes the response to the rotation of the container, and $\lim_{q \rightarrow 0} [\chi^L(\mathbf{q}, 0) - \chi^T(\mathbf{q}, 0)]$ is regarded as the superfluid density ρ_s . (Historically, it is traced back to Schafroth in the study of superconductivity before the advent of BCS theory [22].) When we consider the translational superfluid flow, in view of the continuity to the rotational superfluidity, we will begin with the form $\sigma(\omega = 0) = \rho/(4\eta) = \lim_{q \rightarrow 0} [\chi^L(\mathbf{q}, 0) - \chi^T(\mathbf{q}, 0)]/(4\eta)$.

The Kramers–Kronig relation connects the real and imaginary parts of susceptibility. In the transverse response by $\chi^T(\mathbf{q}, \omega)$, the particle displacements are orthogonal to the external force, thus resulting in the nondissipative response $\omega\sigma_2(\omega)$ in Eq.(35). Hence, the nondissipative part $\omega\sigma_2(\omega) = \omega\rho/(4\eta)$, where $\omega = aq^2$, is represented by $a \int dq^2 \chi^T(\mathbf{q}, \omega)/(4\eta_n)$. (Since we are interested in not only the macroscopic but also a mesoscopic condensate, we integrate $\chi^T(\mathbf{q}, \omega)$ over q , instead of taking $q \rightarrow 0$.) On the other hand, the longitudinal response by $\chi^L(\mathbf{q}, \omega)$ corresponds to the dissipative part $\omega\sigma_1(\omega)$. The Kramers–Kronig relation for Eq.(35) is written as

$$-\omega\sigma_1(\omega) = -\frac{1}{\pi} \frac{1}{4\eta_n} \int_{-\infty}^{\infty} d\xi \int adq^2 \frac{\chi^T(\mathbf{q}, \xi)}{\xi - \omega}. \quad (39)$$

In the coarse-graining ($\mathbf{q} \rightarrow 0$) of a normal liquid, the response to the external force with a larger wavelength becomes more irrelevant to its microscopic structure. Hence, it does not matter in which direction the external force is exerted on the liquid at $\mathbf{q} \rightarrow 0$, with the result that $\lim_{q \rightarrow 0} \chi^L(\mathbf{q}, \omega) = \lim_{q \rightarrow 0} \chi^T(\mathbf{q}, \omega)$ at small ω . Instead of Eq.(39), in analogy to the motion of a rigid body, we usually define the fluidity $\sigma_{1n}(\omega)$ of a normal fluid as

$$\sigma_{1n}(\omega) = \frac{1}{\pi\omega} \frac{1}{4\eta_n} \int_{-\infty}^{\infty} d\xi \int adq^2 \frac{\chi^L(\mathbf{q}, \xi)}{\xi - \omega}. \quad (40)$$

B. Two-fluid model in terms of fluidity spectrum

In a superfluid, the coherent wave function grows to a macroscopic size, and therefore a difference between the longitudinal and transverse properties continues to exist even at $\mathbf{q} \rightarrow 0$, with the result that $\lim_{q \rightarrow 0} \chi^L(\mathbf{q}, \omega) \neq \lim_{q \rightarrow 0} \chi^T(\mathbf{q}, \omega)$. Accordingly, instead of Eq.(40), one must go back to the original definition [Eq.(39)] so that it is applicable to a superfluid. For a superfluid, we rewrite

Eq.(39) as [23]

$$\begin{aligned} \sigma_1(\omega) &= \sigma_{1n}(\omega) \\ &- \frac{1}{\pi\omega} \frac{1}{4\eta_n} \int_{-\infty}^{\infty} d\xi \int adq^2 \frac{\chi^L(\mathbf{q}, \xi) - \chi^T(\mathbf{q}, \xi)}{\xi - \omega} \\ &+ A(T)\delta(\omega). \end{aligned} \quad (41)$$

The second term represents the transition from the normal flow to the superfluid flow. We will obtain $\chi^L(\mathbf{q}, \xi) - \chi^T(\mathbf{q}, \xi)$ using the quantum mechanical many-body theory. We integrate $\chi^L(\mathbf{q}, \omega) - \chi^T(\mathbf{q}, \omega)$ over all possible \mathbf{q} at a given ω in Eq.(41). The third term represents the fluidity of a macroscopic superfluid flow. In a translational superfluid flow, the fluidity is a quantity determined by the fundamental parameters rather than the phenomenological ones such as η_n . In the simplest two-fluid model, one considers only $\sigma_{1n}(\omega)$ and $A(T)\delta(\omega)$ in $\sigma_1(\omega)$.

This is the revised expression of the two-fluid model in terms of the fluidity spectrum. By the spectral analysis of how such a $\chi^L(\mathbf{q}, \omega) - \chi^T(\mathbf{q}, \omega)$ gradually grows with decreasing temperature, we can explore the formation of the translational superfluid flow, which is not seen in the rotational superfluid flow [24] (Appendix D). At the $q \rightarrow 0$ limit, the longitudinal excitation from the condensate is equivalent to the uniform translation of the condensate itself.

IV. PHYSICAL MODEL OF TRANSLATIONAL SUPERFLUID FLOW

On the basis of the physical view in Sec 2, let us consider the fluidity spectrum $\sigma_1(\omega)$ of the superfluid flow in liquid.

(1) In a slowly moving Bose system in which the physical quantities slowly vary in space and time, we can regard the system as a mixture of some local equilibrium states, and therefore the first approximation of $\chi_{\mu\nu}(\mathbf{q}, \omega)$ is one-particle excitations from the condensate (the zeroth order of U) given by

$$\begin{aligned} \chi_{\mu\nu}(\mathbf{q}, \omega) &= - \sum_p \hbar^2 \left(p + \frac{q}{2} \right)_\mu \left(p + \frac{q}{2} \right)_\nu \\ &\times \frac{f_B(p) - f_B(p+q)}{\hbar\omega + \epsilon(p) - \epsilon(p+q)}, \end{aligned} \quad (42)$$

where $f_B(p)$ is the Bose distribution function.

In view of $\chi_{\mu\nu}(\mathbf{q}, \omega)$ in Eq.(38), $\chi^L(\mathbf{q}, \omega) - \chi^T(\mathbf{q}, \omega)$ is the coefficient of $q_\mu q_\nu/q^2$. Hence, in the case of Eq.(42), we obtain

$$\begin{aligned} [\chi^L(\mathbf{q}, \omega) - \chi^T(\mathbf{q}, \omega)] \frac{q_\mu q_\nu}{q^2} \\ = -\frac{\hbar^2}{4} \sum_p \frac{f_B(p) - f_B(p+q)}{\hbar\omega + \epsilon(p) - \epsilon(p+q)} q^2 \times \frac{q_\mu q_\nu}{q^2}. \end{aligned} \quad (43)$$

When viewing the superfluid flow at $T = 0K$ on a reference frame moving at a momentum p , the system consists of various coherent wave functions having zero momentum ($p = 0$), and we can simplify the sum over p by putting $f_B(p) = 0$ for a finite p . While a capillary flow is originally a dissipative process, time-reversal symmetry holds for $\chi^L(\mathbf{q}, \omega) - \chi^T(\mathbf{q}, \omega)$ in the Kramers–Kronig relation of Eq.(41). Hence, we consider in Eq.(43), not only a term with $p = 0$ representing an excitation $\epsilon(0) \rightarrow \epsilon(q)$ from the condensate, but also a term with $p = -q$ representing a decay $\epsilon(-q) \rightarrow \epsilon(0)$ to the condensate. The former corresponds to $\epsilon(p) - \epsilon(p+q) \simeq -\hbar^2 q^2 / (2m) \equiv -\hbar a q^2$, where $a = \hbar / (2m)$, and the latter to $\epsilon(p) - \epsilon(p+q) \simeq \hbar^2 q^2 / (2m) = \hbar a q^2$. Hence, we find that

$$\chi^L(\mathbf{q}, \omega) - \chi^T(\mathbf{q}, \omega) = -\frac{\hbar}{4} \left(\frac{f_B(0)}{\omega - a q^2} + \frac{-f_B(0)}{\omega + a q^2} \right) q^2. \quad (44)$$

(When ω is defined in $-\infty < \omega < \infty$, the first and second terms have the same form.)

(2) To improve $\chi_{\mu\nu}(\mathbf{q}, \omega)$ so that it reflects the situation of the liquid, we construct the longitudinal and transverse susceptibilities by comparing Eqs.(38) and (42). Since the transverse excitation energy depends on the size of the coherent wave function, we decompose $f_B(p = 0)$ in Eq.(44) into a sum over s using $h(s) = \exp(\beta\mu s)/s$ for $p = 0$ [25]. Such a $\chi_{\mu\nu}(\mathbf{q}, \omega)$ at a low frequency in $-\infty < \omega < \infty$ is given by

$$\begin{aligned} \chi_{\mu\nu}(\mathbf{q}, \omega) &= \sum_s^\infty sh(s) \frac{\hbar}{2} \frac{-q^2}{\omega - a_l q^2} \frac{q_\mu q_\nu}{q^2} \\ &+ \sum_s^\infty sh(s) \frac{\hbar}{2} \frac{-q^2}{\omega - \epsilon_t(s, q)/\hbar} \left(\delta_{\mu\nu} - \frac{q_\mu q_\nu}{q^2} \right), \end{aligned} \quad (45)$$

where q is mainly a wave vector along the flow direction. The excitation energy $\epsilon_t(s, q)$ of the transverse motion depends on the size s of the coherent wave function: (a) $\epsilon_t(s, q) = \epsilon_0$ for excitations within the coherent wave function as in Eq.(16), and (b) $\epsilon_t(s, q) = \hbar a_t q^2$ for that beyond the coherent wave function as shown in Fig.4 [26]. We distinguish the longitudinal one-particle excitation energy $\epsilon(p+q) - \epsilon(p) = \hbar^2 / (2m_l) \times q^2 = \hbar a_l q^2$ from that of the transverse one $\hbar^2 / (2m_t) \times q^2 = \hbar a_t q^2$.

A new form of $\sigma_1(\omega)$ is obtained using Eq.(45) as follows. Extracting $\chi^L(\mathbf{q}, \omega) - \chi^T(\mathbf{q}, \omega)$ from Eq.(45) by comparing it with Eq.(38), and substituting this result in Eq.(41), we obtain the fluidity spectrum

$$\begin{aligned} \sigma_1(\omega) &= \sigma_{1n}(\omega) + \frac{\hbar}{2\pi} \frac{1}{4\eta_n} a \int dq^2 \frac{q^2}{\omega} \sum_s^\infty sh(s) \int_{-\infty}^\infty d\xi \\ &\times \frac{1}{\xi - \omega} \left(\frac{1}{\xi - a_l q^2} - \frac{1}{\xi - \epsilon_t(s, q)/\hbar} \right) \\ &+ A(T)\delta(\omega). \end{aligned} \quad (46)$$

Defining a new variable $x = \xi - a q^2$ in the above integral, we can use the Hilbert transformation of $1/x$, which is another form of $1/(x + i\epsilon) = 1/x - i\pi\delta(x)$,

$$\frac{1}{\pi} \int_{-\infty}^\infty \frac{dx}{x - \omega} \frac{1}{x} = \pi\delta(\omega). \quad (47)$$

Applying the Hilbert transformation, we obtain

$$\begin{aligned} \sigma_1(\omega) &= \sigma_{1n}(\omega) \\ &+ \frac{\pi\hbar}{2} \frac{1}{4\eta_n} a \int dq^2 \\ &\times \sum_s^\infty sh(s) \frac{q^2}{\omega} [\delta(\omega - a_l q^2) - \delta(\omega - \epsilon_t(s, q)/\hbar)] \\ &+ A(T)\delta(\omega). \end{aligned} \quad (48)$$

$\delta(\omega - a_l q^2)$ and $\delta(\omega - \epsilon_t(s, q)/\hbar)$ represent the contributions from the longitudinal and transverse excitations, being the result of the first and second terms in Eq.(20), and the third term in it, respectively. [$\sigma_{1n}(\omega)$ includes more complex phenomena than that in Eq.(45). However, we focus on the change in $\sigma_1(\omega)$ near T_λ , hence assuming that this change is well described by the simple $\chi_{\mu\nu}(\mathbf{q}, \omega)$ such as Eq.(45).]

A. $\sigma_1(\omega)$ from the transverse motion

According to the mechanism explained in Fig.4, the sum over s in the transverse motion in Eq.(48) is divided into two parts: a sum ($s > s_1$) in which excitations occur within the same coherent wave function and the statistical gap ϵ_0 suppresses the transverse excitations, and a sum ($s < s_1$) in which excitations occur beyond the coherent wave function and permutation symmetry no longer restricts the transverse excitations of the system.

$$\begin{aligned} &\sum_{s=1}^\infty s h(s) \frac{q^2}{\omega} \delta(\omega - \epsilon_t(s, q)/\hbar) \\ &= \sum_{s=1}^{s_1} sh(s) \frac{q^2}{\omega} \delta(\omega - a_t q^2) + \sum_{s=s_1+1}^\infty sh(s) \frac{q^2}{\omega} \delta(\omega - \epsilon_0/\hbar) \end{aligned} \quad (49)$$

The boundary size s_1 between these sums is determined as follows. As schematically illustrated in Fig.4, the wavelength $2\pi/q$ of the transverse excitation with $\omega = a_t q^2$ slightly exceeds the length of the condensate R_{\parallel} at s_1 . Here, we apply the model calculation described in Sec 2B to this condition, that is, in the ellipsoid with a volume $(4\pi/3)R_{\parallel}R_{\perp}^2 = sr_0^3$ in which $R_{\parallel} = s^2 r_0$, this s_1 is determined by $R_{\parallel} = 2\pi/q$: that is, $s_1^2 r_0 = 2\pi/\sqrt{\omega/a_t}$, hence

$$s_1 = \left(\frac{2\pi}{r_0} \sqrt{\frac{a_t}{\omega}} \right)^{1/2}. \quad (50)$$

On the right-hand side of Eq.(49), since $\hbar\omega \ll \epsilon_0$ in experiments, we can ignore the second term. In the first term, at every q , a sum over s from 1 to s_1 is calculated, in such a way that the transverse excitation beyond the coherent wave function has an energy of $a_t q^2$. Putting Eq.(49) into Eq.(48), and integrating it over q^2 while keeping q^2/ω fixed, the summation over s using $sh(s) = \exp(\beta\mu s)$ yields

$$\begin{aligned} & a \int dq^2 \sum_{s=1}^{s_1} sh(s) \frac{q^2}{\omega} \delta(\omega - a_t q^2) \\ &= -\frac{a}{a_t^2} \sum_{s=1}^{s_1} \exp(\beta\mu s) = -\frac{a}{a_t^2} f_B(0, T) [1 - \exp(\beta\mu s_1)]. \end{aligned} \quad (51)$$

At $\omega = 0$, since $s_1 = \infty$ in Eq.(50), the transverse motion makes a finite contribution to $\sigma_1(\omega)$ as $-(a/a_t^2)f_B(0, T)$ in Eq.(51), but does not produce a $\delta(\omega)$ peak.

B. $\sigma_1(\omega)$ from the longitudinal motion

A superfluid flow, which is the translational motion of a macroscopic condensate, is the $q \rightarrow 0$ limit of the longitudinal oscillation. Originally, it does not directly depend on the viscosity η_n . Rather, it is determined by the basic parameters, although it is indirectly related to η_n by the sum rule [Eq.(15)]. Hence, in view of the dimension of $\sigma_1(\omega)$, and the experimental result that the flow rate of a superfluid flow is inversely proportional to d^2 , rather than L , we assume the general form $\tilde{A}(T)(\pi/d^2)\delta(\omega)$, and will determine a dimensionless quantity $\tilde{A}(T)$ using the sum rule [21]. On the other hand, for the longitudinal motion observed at $\omega \neq 0$ in Eq.(48), there is no boundary size s_1 in the sum over s . Hence, we obtain

$$\begin{aligned} & a \int dq^2 \sum_{s=1}^{\infty} sh(s) \frac{q^2}{\omega} \delta(\omega - a_l q^2) \\ &= -\frac{a}{a_l^2} \sum_{s=1}^{\infty} \exp(\beta\mu s) = -\frac{a}{a_l^2} f_B(0, T). \end{aligned} \quad (52)$$

C. Total $\sigma_1(\omega)$

Substituting Eqs.(51) and (52) into the integrand of Eq.(48), we obtain

$$\begin{aligned} & a \int dq^2 \sum_{s=1}^{\infty} sh(s) \frac{q^2}{\omega} \\ & \times [\delta(\omega - a_l q^2) - \delta(\omega - \epsilon_t(s, q)/\hbar)] \\ &= f_B(0, T) \left[-\frac{a}{a_l^2} + \frac{a}{a_t^2} - \frac{a}{a_t^2} \exp(\beta\mu s_1) \right]. \end{aligned} \quad (53)$$

Using Eq.(53) in Eq.(48), we finally obtain the fluidity spectrum

$$\begin{aligned} \sigma_1(\omega) &= \sigma_{1n}(\omega) + \tilde{A}(T) \frac{\pi}{d^2} \delta(\omega) + \frac{\hbar}{2m} \pi \frac{\rho_s(T)}{4\eta_n} \\ & \times \left[\frac{a}{a_t^2} - \frac{a}{a_l^2} - \frac{a}{a_t^2} \exp \left(\beta\mu(T) \left[\frac{2\pi}{r_0} \sqrt{\frac{a_t}{\omega}} \right]^{1/Z} \right) + \frac{a}{a_l^2} \right] \end{aligned} \quad (54)$$

where Eq.(50) is used for s_1 , and $\rho_s(T) = m f_B(0, T)$ is used for the small but nonzero condensate already existing just above T_λ (m is the conventional mass in thermodynamic quantities). In this result, the last a/a_l^2 is added in the bracket of the third term, in order to ensure $\sigma_1(\omega) \rightarrow 0$ at $\omega \rightarrow \infty$. Using $a = \hbar/(2m)$ and $\epsilon_0 = \hbar a_t/r_0^2$ for the transverse motion, we rewrite Eq.(54) as

$$\begin{aligned} \sigma_1(\omega) &= \sigma_{1n}(\omega) + \tilde{A}(T) \frac{\pi}{d^2} \delta(\omega) \\ & + \pi \frac{m_t^2}{m^2} \frac{\rho_s(T)}{4\eta_n} \\ & \times \left[1 - \exp \left(\beta\mu(T) \left[\sqrt{(2\pi)^2 \frac{m}{m_t} \frac{\epsilon_0}{\hbar\omega}} \right]^{1/Z} \right) \right]. \end{aligned} \quad (55)$$

[For liquid helium 4, $(2\pi)^2 \epsilon_0/\hbar\omega \simeq 1.11 \times 10^{14}/\omega$.]

Equation (55) is a microscopic representation of the change from $\sigma(\omega)$ to $\sigma_s(\omega) + A\delta(\omega)$ in Fig.2. If the statistical gap does not exist in the transverse excitation, only the first and second terms remain on the right-hand side of Eq.(55), which reduces to the simplest two-fluid model representing the discontinuous appearance of a superfluid flow. Hence, the statistical gap ϵ_0 is necessary for the continuous growth of a superfluid flow. Although ϵ_0 itself does not explicitly appear in $\tilde{A}(T)(\pi/d^2)\delta(\omega)$, the statistical gap controls the superfluid flow behind the scenes.

D. $\sigma_{1n}(\omega)$ from normal-fluid component

The two-fluid picture gives us the fluid-mechanical equation by rewriting Eq.(1) with $\rho = \rho_n(T) + \rho_s(T)$ and $\mathbf{v} = \mathbf{v}_n(T) + \mathbf{v}_s(T)$ as

$$\rho_n \frac{\partial \mathbf{v}_n}{\partial t} + \rho_s \frac{\partial \mathbf{v}_s}{\partial t} = \eta \nabla^2 \mathbf{v}_n - \nabla P. \quad (56)$$

Since \mathbf{v}_s is a potential flow as $\mathbf{v}_s = \nabla \phi$, where ϕ is a potential function, we obtain the equation of \mathbf{v}_n as

$$\rho_n \frac{\partial \mathbf{v}_n}{\partial t} = \eta \nabla^2 \mathbf{v}_n - \nabla P_n, \quad (57)$$

where P_n is the pressure acting on the normal-fluid component

$$P_n = P + \rho_s(T) \frac{\partial \phi}{\partial t}. \quad (58)$$

Following the Newtonian equation of motion, the superfluid flow is accelerated under pressure P_0 at $z = 0$ as

$$v_s = \left(\frac{P_0 \pi d^2}{m} \right) t, \quad (59)$$

and therefore the potential function in $\mathbf{v}_s = \nabla\phi$ has the form

$$\phi(z, t) = \left(\frac{P_0 \pi d^2}{m} \right) tz. \quad (60)$$

Instead of the original pressure gradient P/L given by $P(z) = P_0(1 - bz)$, by using Eq.(60) in Eq.(58), we find that the normal-fluid component in liquid experiences a different pressure of

$$P_n(z) = P_0 \left(1 - \left[b - \rho_s(T) \frac{\pi d^2}{m} \right] z \right). \quad (61)$$

In Eq.(57), the pressure gradient takes a form such as

$$\nabla P_n = \left[1 - \rho_s(T) \left(\frac{\pi d^2}{bm} \right) \right] \nabla P \equiv [1 - \rho_s(T)f] \nabla P. \quad (62)$$

The mass transport by the superfluid flow reduces the pressure gradient acting on the normal-fluid component. Hence, as a solution of Eq.(57), the fluidity spectrum $\sigma_{1n}(\omega)$ of the normal-fluid component is given by

$$\sigma_{1n}(\omega) = - \left(\frac{1 - \rho_s(T)f}{\omega d^2} \right) \times \text{Im} \left(1 - \frac{1}{J_0 \left(id[1 - i] \sqrt{\frac{\rho_n(T)}{2\eta_n} \omega} \right)} \right) \quad (63)$$

E. Sum rule

The change in $\sigma_1(\omega)$ near T_λ must satisfy the sum rule. Using Eq.(8) for $\sigma(\omega)$ on the left-hand side of Eq.(15), and using Eqs.(55) and (63) for $\sigma_s(\omega) + A\delta(\omega)$ on the

right-hand side, we obtain the sum rule

$$\begin{aligned} \tilde{A}(T) \frac{\pi}{d^2} + \pi \frac{\rho_s(T)}{4\eta_n} 2 \frac{m_t^2}{m^2} \int_0^\infty d\omega \\ \times \left[1 - \exp \left(\beta\mu(T) \left[\sqrt{(2\pi)^2 \frac{m}{m_t} \frac{\epsilon_0}{\hbar\omega}} \right]^{1/Z} \right) \right] \\ = 2 \int_0^{\omega_c} \frac{d\omega}{\omega d^2} \text{Im} \left(\frac{1}{J_0 \left(id[1 - i] \sqrt{\frac{\rho}{2\eta_n} \omega} \right)} \right) \\ - 2 \int_0^{\omega_c} \frac{d\omega}{\omega d^2} \text{Im} \left(\frac{1 - f\rho_s(T)}{J_0 \left(id[1 - i] \sqrt{\frac{\rho_n(T)}{2\eta_n} \omega} \right)} \right), \end{aligned} \quad (64)$$

where $\rho_n(T) + \rho_s(T) = \rho$. Whereas the right-hand side of Eq.(64) comes from fluid mechanics including phenomenological parameters, the left-hand side comes from the microscopic many-body theory. This sum rule for a liquid can be regarded as a dynamic version of the equation of states of the ideal Bose gas

$$\frac{1}{V} \frac{z}{1 - z} + \frac{1}{\lambda^3} g_{3/2}(z) = \frac{N}{V} \quad (65)$$

[$z = \exp(\beta\mu)$, and λ is the thermal wavelength]. Both equations determine the static or dynamic representation of a superfluid by the conservation law.

Historically, the striking finding of superfluidity was a discovery of a frictionless flow with $\eta = 0$. However, its more essential feature is not $\eta = 0$, but the constraint $\text{rot}\mathbf{v}_s = 0$ on the superfluid flow [3]. Equation (64) supports this view as follows. The existence of the statistical gap ϵ_0 , which forbids transverse motion such as $\text{rot}\mathbf{v}_s = 0$, induces the change in $\sigma_1(\omega)$. As a result, $\tilde{A}(T)(\pi/d^2)\delta(\omega)$ representing the frictionless flow $\eta = 0$ inevitably appears so as to satisfy the sum rule.

(1) For the right-hand side of Eq.(64), fluid mechanics does not describe oscillations with high frequency, because a liquid shows solidlike properties at a high frequency [4]. Hence, we cannot extend the upper end of the integral to ∞ and assume a cutoff frequency ω_c .

(2) The effect of a repulsive interaction on the superfluid flow is unclear. Hence, in the model calculation in Sec 5, we will assume no renormalization of the mass $m_t = m_l = m$ as a first approximation, and determine $\tilde{A}(T)$ of the superfluid flow so that Eq.(64) is satisfied at each temperature.

V. MODEL CALCULATION OF FLUIDITY SPECTRUM

Experimentally, we observe a seemingly vertical drop of $\nu(T) = 1/(4\sigma(T))$ at T_λ as in Fig.1. If we could put

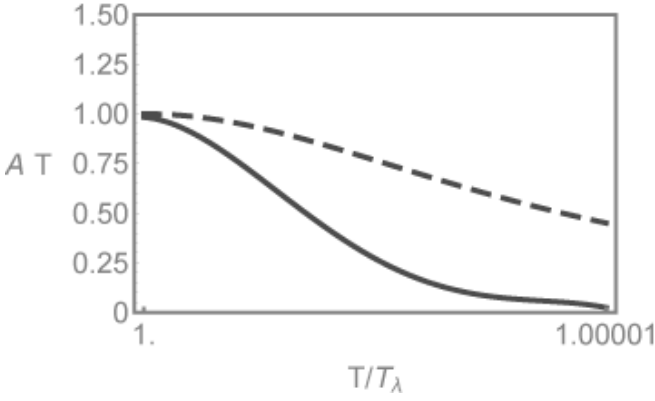


FIG. 6: Growth of superfluid flow $\tilde{A}(T)$ (thick curve) just above T_λ for (a) $\rho_s(T_\lambda)/\rho = 1.00$ and $Z = 1$. The dashed curve shows $\rho_s(T)/\rho$.

our thought experiment into practice under the precise control of temperature and suppress the fluctuation near T_λ , we could observe the growth of a superfluid flow as a change in the fluidity spectrum $\sigma_1(\omega)$. All the results in Sec.5 are obtained so that they satisfy the sum rule in Eq.(64).

In comparison with a gas, a strongly coupled system such as a liquid has more excitations with low energy. Hence, the temperature dependence of $\mu(T)$ in a liquid is weaker than $\mu_0(T)$ in a gas. However, the chemical potential $\mu(T)$ of liquid helium 4 just above T_λ has not yet derived from experiment and theory. When we use $\mu_0(T)$ [Eq.(24)] of the ideal Bose gas as $\mu(T)$ in $h(s)$, such a $h(s)$ extends to a large s only after T becomes extremely close to $2.17K$. Because of these reasons, ambiguity remains in our model calculation of the fluidity spectrum for liquid helium 4 [27]. Rather, to demonstrate the mechanism in Fig.4 without ambiguity, we perform a model calculation of it at extremely close T to $2.17K$.

We are interested in the effect of the repulsive interaction U_0 on the superfluid flow through different $\rho_s(T)/\rho$. Numerically, we adopt a definition $\rho_s(T)/\rho = \hat{f}_B(0, T)/\hat{f}_B(0, T_\lambda)$ in which U_0 in $\hat{f}_B(0, T)$ and U'_0 in $\hat{f}_B(0, T)$ are different. By changing U_0/U'_0 , we control $\rho_s(T)/\rho$. We are also interested in the effect of the degree of elongation Z of the coherent wave function on the fluidity spectrum. We assumed an elongated form of the coherent wave function in the flow as $R_{\parallel} \simeq s^Z r_0$. In summary, we consider three cases: (a) $\rho_s(T_\lambda)/\rho = 1.00$ and $Z = 1$, (b) $\rho_s(T_\lambda)/\rho = 0.56$ and $Z = 1$, and (c) $\rho_s(T_\lambda)/\rho = 1.00$ and $Z = 0.9$, by assuming $U_0/U'_0 = 1.0$ for (a) and (c) and $U_0/U'_0 = 1.8$ for (b).

Other parameters used are as follows. In the normal phase of liquid helium 4, we have $\rho = 1.43 \times 10^2$ [kg/m³] and $\eta_n = 3.0 \times 10^{-6}$ [Js/m³]: hence, $\rho/(4\eta_n) = 1.2 \times 10^7$ [s/m²]. In Eq.(64), $d = 1mm$, $\omega_c = 0.6s^{-1}$ and $f = \pi d^2/(bm) = 0.1$ are used.

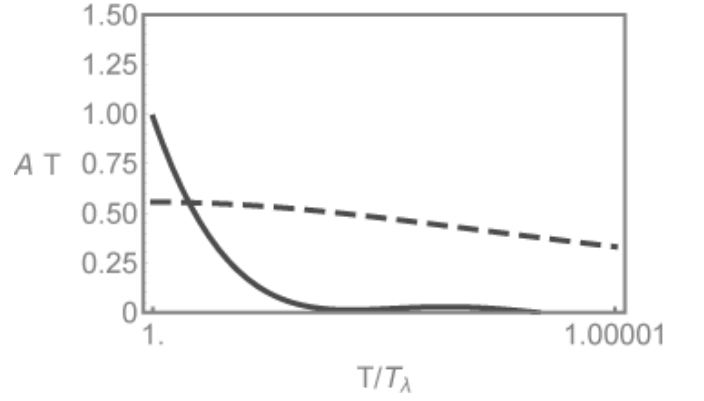


FIG. 7: Growth of superfluid flow $\tilde{A}(T)$ (thick curve) just above T_λ for (b) $\rho_s(T_\lambda)/\rho = 0.56$ and $Z = 1$. The dashed curve shows $\rho_s(T)/\rho$.

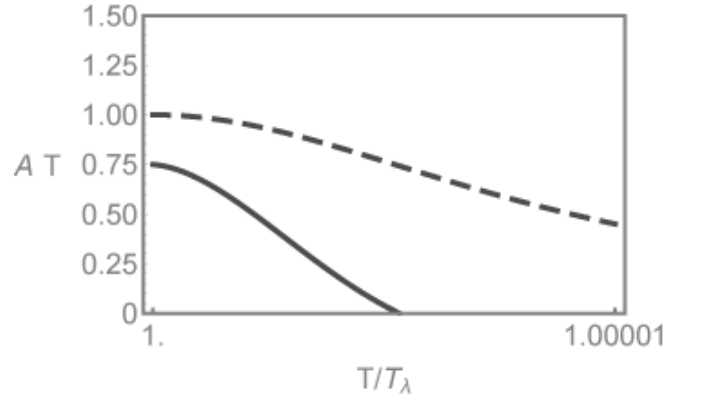


FIG. 8: Growth of superfluid flow $\tilde{A}(T)$ (thick curve) just above T_λ for (c) $\rho_s(T_\lambda)/\rho = 1.00$ and $Z = 0.9$. The dashed curve shows $\rho_s(T)/\rho$.

A. Growth of superfluid flow just above T_λ

The rate of the superfluid flow $\tilde{A}(T)$ in $\tilde{A}(\pi/d^2)\delta(\omega)$ just above T_λ is determined as a function of T/T_λ so as to satisfy the sum rule Eq.(64). Figure 6 shows $\tilde{A}(T)$ just above T_λ (thick curve) for (a) $\rho_s(T_\lambda)/\rho = 1.00$ and $Z = 1$, in comparison with $\rho_s(T)/\rho$ (dashed curve). Figure 7 shows $\tilde{A}(T)$ just above T_λ for (b) $\rho_s(T_\lambda)/\rho = 0.56$ and $Z = 1$, in comparison with $\rho_s(T)/\rho$. For both (a) and (b), $\tilde{A}(T)$ grows more rapidly than $\rho_s(T)/\rho$ near T_λ . In the case of (b) for $\rho_s(T_\lambda)/\rho = 0.56$, $\rho_s(T)/\rho$ remains smaller than 1, but $\tilde{A}(T)$ finally rises to 1 at T_λ . In view of these results, the thermodynamic rate of the superfluid density $\rho_s(T)/\rho$ and the rate of the translational superfluid flow $\tilde{A}(T)$ are different quantities.

Figure 8 shows $\tilde{A}(T)$ and $\rho_s(T)/\rho$ for (c) $\rho_s(T_\lambda)/\rho = 1.00$ and $Z = 0.9$. If we assume a more isotropic form of the coherent wave function in the flow by reducing Z in $s^Z r_0$, the effective length R_{\parallel} of the coherent wave

function in Fig.4 is reduced in comparison with the case of $Z = 1$ at the same temperature. Hence, $\tilde{A}(T)$ does not reach 1 at T_λ .

B. Precursory form of superfluid flow in the increase in $\sigma_1(\omega)$ near $\omega = 0$

Using the third term on the right-hand side of Eq.(55), $\sigma_1(\omega)$ near $\omega = 0$ is plotted. Figure 9 shows the continuous increase in $\sigma_1(\omega)$ near $\omega = 0$ for (a) $\rho_s(T_\lambda)/\rho = 1.00$ and $Z = 1$ just above T_λ . [$\sigma_{1n}(\omega)$ is not included.] This temperature dependence comes from $\mu(T)$ in the exponent and $\rho_s(T)$. At $1.00003T_\lambda$, the peak at $\omega = 0$ has not yet appeared, because only the small coherent wave function contributes to $\sigma_1(\omega)$. At $1.00002T_\lambda$, a small peak at $\omega = 0$ appears. As $T \rightarrow T_\lambda$, the effect of the statistical gap gradually accumulates in $\sigma_1(\omega)$ at low frequencies, finally becoming the $\delta(\omega)$ -function peak representing a superfluid flow. The abrupt change in $\sigma_1(\omega)$ just above T_λ in Fig.9 is consistent with the observed vertical drop of ν in Fig.1. Since s_1 in Eq.(50), determining the ω dependence of $\sigma_1(\omega)$ near $\omega = 0$, does not depend on $\rho_s(T)/\rho$, the continuous increase in $\sigma_1(\omega)$ near $\omega = 0$ for (b) just above T_λ is similar to that of (a). However, since s_1 depends on Z , $\sigma_1(\omega)$ near $\omega = 0$ for (c) $Z = 0.9$ is considerably different from those of (a) and (b).

The increase in $\sigma_1(\omega)$ at small ω in Eq.(48) is due to excitations with a large wavelength λ for $q = 2\pi/\lambda$ in $\delta(\omega - aq^2)$. Hence, in the sum over s in Eq.(49) at small ω , a difference between the longitudinal and transverse excitations continue to exist from a small to large s , thereby leading to a large $\sigma_1(\omega)$ near $\omega = 0$. In contrast, $\sigma_1(\omega)$ at large ω is due to excitations with a small wavelength. Hence, the difference between both excitations exists only for small s in the sum, hence leading to a small $\sigma_1(\omega)$. Just above T_λ , the approach of $\mu(T)$ to zero as $T \rightarrow T_\lambda$ in the exponent of Eq.(55) represents the growth of the condensate, hence leading to the inclusion of a long excitation in $\sigma_1(\omega)$, as schematically illustrated in Fig.4. The exponent in Eq.(55) shows this mechanism at different temperatures. The third term in Eq.(55) has a comparable value with the first term $\sigma_{1n}(\omega)$ only at $\omega \simeq 0$. For larger ω , it rapidly falls owing to the exponential factor, and only $\sigma_{1n}(\omega)$ remains in $\sigma_n(\omega)$.

C. $\sigma_{1n}(\omega)$ of normal-fluid component

When the $\delta(\omega)$ -function peak begins to rise when cooling the system, $\sigma_1(\omega)$ is still composed of $\sigma_{1n}(\omega)$ of the normal-fluid component. This $\sigma_{1n}(\omega)$ in Eq.(63) depends on not only ρ/η , but also the radius d of the capillary. Figure 10 shows the temperature change of $\sigma_{1n}(\omega)$ in Eq.(63) for (a) and (c) in the case of $f = 0.1$ and $d = 1$ [mm]: The $\sigma_{1n}(\omega)$ at $T \gg T_\lambda$ (thick curve) changes to $\sigma_{1n}(\omega)$ at $1.00001T_\lambda$ (one-point dotted curve) and $\sigma_{1n}(\omega)$ at $1.000005T_\lambda$ (short dotted curve), and finally reaches

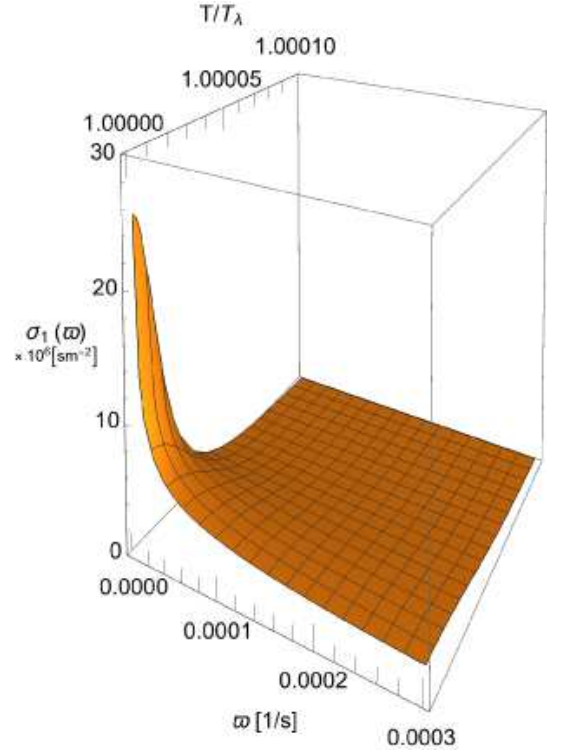


FIG. 9: Continuous increase in the fluidity spectrum $\sigma_1(\omega)$ near $\omega = 0$ along the axis of capillary when approaching T_λ in the oscillatory Poiseuille's flow. The third term in Eq.(55) is plotted for (a) $\rho_s(T_\lambda)/\rho = 1.00$ and $Z = 1$. [$\sigma_{1n}(\omega)$ is not included.]

$\sigma_{1n}(\omega)$ at $1.000003T_\lambda$ (long dotted curve). Throughout this change, the upper-convex form of $\sigma_{1n}(\omega)$ near $\omega = 0$ is maintained, which is a characteristic feature of a normal fluid.

D. Total fluidity spectrum $\sigma_1(\omega)$

Finally, we obtain a more precise form of $\sigma_s(\omega) + A\delta(\omega)$, which was schematically illustrated in Fig.2, by combining the microscopic and phenomenological methods.

Figure 11 shows the total fluidity spectrum $\sigma_1(\omega)$ in Eq.(55) for (a) $\rho_s(T_\lambda)/\rho = 1.00$ and $Z = 1$ at four different temperatures just above T_λ under the same parameters used in Fig.9. The thick upper-convex curve shows $\sigma_{1n}(\omega)$ in the normal phase at $T \gg T_\lambda$ [Eq.(8)] (thick curve in Fig.10). As $T \rightarrow T_\lambda$, $\sigma_1(\omega)$ continuously changes as follows. The one-point dotted curve at $1.00001T_\lambda$ has already lost the upper-convex form near $\omega = 0$, which transforms to a lower-convex one. Upon cooling to $1.0000055T_\lambda$, the short dotted curve of $\sigma_1(\omega)$ appears. Finally, the long dotted curve of $\sigma_1(\omega)$ appears at $1.000003T_\lambda$ just above T_λ . Similarly, Fig.12 shows the continuous change in the total fluidity spectrum $\sigma_1(\omega)$ for (b) $\rho_s(T_\lambda)/\rho = 0.56$ and $Z = 1$, in which $\sigma_{1n}(\omega)$ of

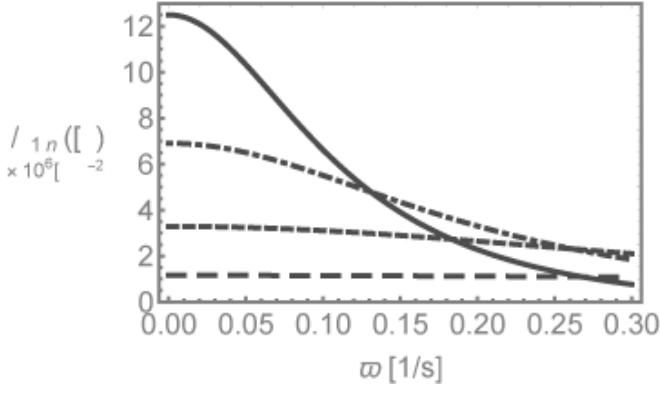


FIG. 10: Fluidity spectrum $\sigma_{1n}(\omega)$ of normal-fluid component just above T_λ in the oscillatory Poiseuille's flow for (a). Equation (63) is plotted in the case of $f = 0.1$ and $d = 1mm$, with ρ_n at $T \gg T_\lambda$ (thick curve), ρ_n at $1.00001T_\lambda$ (one-point dotted curve), ρ_n at $1.0000055T_\lambda$ (short dotted curve), and ρ_n at $1.000003T_\lambda$ (long dotted curve).

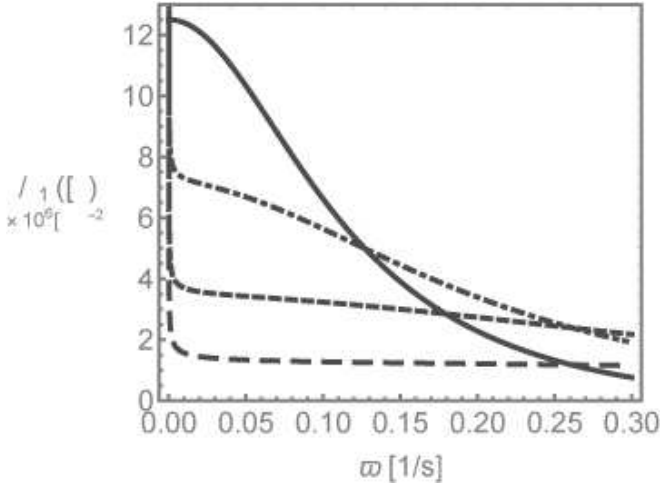


FIG. 11: Continuous change in the total fluidity spectrum $\sigma_1(\omega)$ when approaching T_λ . They are calculated using Eq.(55), in which $\tilde{A}(T)$ satisfies Eq.(64), for (a) $\rho_s(T_\lambda)/\rho = 1.00$ and $Z = 1$. The thick upper-convex curve shows $\sigma_{1n}(\omega)$ in the normal phase at $T \gg T_\lambda$ (Fig.10). The one-point dotted curve appears at $1.00001 T_\lambda$. In the short dotted curve at $1.0000055 T_\lambda$, the upper-convex nature near $\omega = 0$ has already disappeared. At $1.000003 T_\lambda$, just above T_λ , this $\sigma_1(\omega)$ changes to the long dotted curve.

the normal-fluid component still remains just above T_λ .

The fluidity $\sigma_1(\omega)$ near $\omega = 0$ changes its form from an upper-convex form to a lower-convex one. The upper-convex form of $\sigma_1(\omega)$ means that the classical liquid is robust when the applied pressure slowly oscillates. This is because the viscous flow itself contains oscillations with various low frequencies. Such an upper-convex form of $\sigma_1(\omega)$ in the viscous flow continuously changes to a lower-

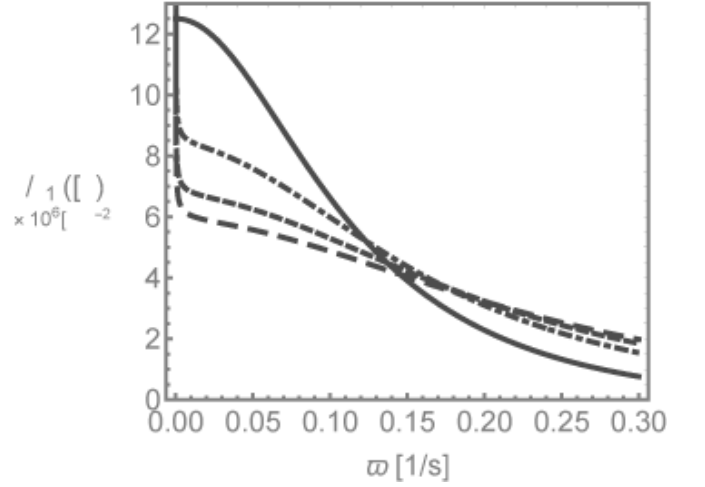


FIG. 12: Continuous change in the total fluidity spectrum $\sigma_1(\omega)$ when approaching T_λ , for (b) $\rho_s(T_\lambda)/\rho = 0.56$ and $Z = 1$.

convex one in the superfluid flow. The lower-convex form means that the superfluid flow is very fragile when the applied pressure oscillates. This is because the superfluid flow is an one-directional motion not including oscillations.

Until now in this paper, we have been considering the thought experiment in which an oscillatory pressure is intentionally applied to a superfluid flow, but if it is accidentally applied to a superfluid flow, we will have a different impression on the result. When the flow velocity increases, the friction against the wall of the capillary yields the local oscillation of liquid, thus inducing pressure oscillation with a low frequency. The lower-convex form of $\sigma_1(\omega)$ in Figs.11 and 12 indicates that even if the pressure only slightly oscillates, it substantially destroys the superfluid flow, hence giving us a new interpretation of the critical velocity v_c of a superfluid flow at $T < T_\lambda$. This suppression is different from the well-known mechanism of the critical superfluid velocity owing to the formation of a vortex ring [28]. To predict a concrete value of v_c , however, we must have a microscopic theory of the friction arising between the wall of a capillary and the flowing liquid.

Figure 13 shows the total fluidity spectrum $\sigma_1(\omega)$ for (c) $Z = 0.9$. When $Z = 0.9$ in Eq.(50), the same ω corresponds to a larger s_1 compared with the case of $Z = 1$. Hence, a large coherent wave function contributes to $\sigma_1(\omega)$ compared with the case of $Z = 1$. The increase in $\sigma_1(\omega)$ is not localized to $\omega \simeq 0$. The transformation of $\sigma_1(\omega)$ to $\sigma_s(\omega) + A\delta(\omega)$ comes not only from $\sigma_{1n}(\omega)$ in Fig.10, but also from the third term in Eq.(55).

In response to the slowly varying external perturbation, the strongly interacting particles with high density, such as those in a liquid, reaches a local equilibrium at each instant. Hence, the system is described by a

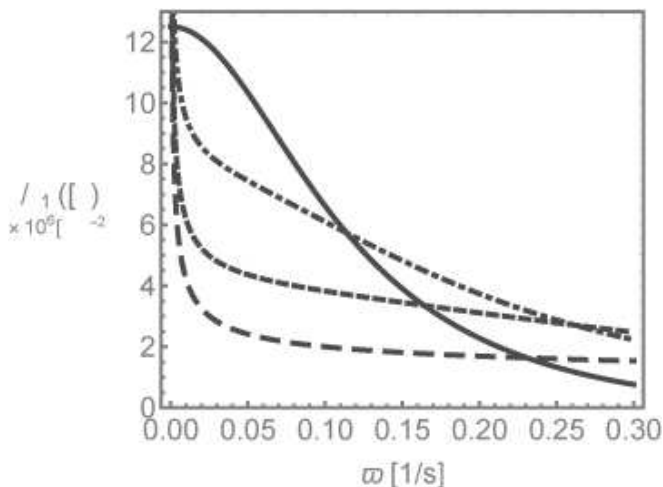


FIG. 13: Continuous change in the total fluidity spectrum $\sigma_1(\omega)$ when approaching T_λ , for (c) $\rho_s(T_\lambda)/\rho = 1.00$ and $Z = 0.9$.

small number of local equilibrium variables, and the fluid-mechanical description becomes a useful tool for such a system. Compared with this general trend, the reason why the Bose condensate, although being a macroscopic system, has only a small number of variables is found in a unique mechanism. By suppressing other excitations, Bose statistics enhances the role of one-particle excitations from the condensate, which also has only a small number of variables. In the transformation of the upper-convex $\sigma_1(\omega)$ to the lower-convex $\sigma_1(\omega)$ in Figs.11–13, we see a transition from one mechanism to another in reducing the number of variables of the macroscopic systems.

VI. DISCUSSION

The following intuitive explanation for the result of this paper is possible. In analogy to the shear transformation of solids, Maxwell related the shear viscosity η of a liquid to the relaxation time τ of the dissipative process in the liquid by $\eta = G\tau$, where G is the modulus of rigidity of the liquid (Maxwell's relation [29]). The relaxation time τ is related to the energy difference $E - E_0$ before and after the relaxation as $\hbar/\tau \propto |E - E_0|$. Hence, the statistical gap in $|E - E_0|$ leads to the decrease in τ , then leading to the decrease in η . In this paper, we formulated this intuitive explanation in the framework of statistical mechanics.

A. Comparison with superconductivity

In superconductivity, a sum rule similar to Eq.(15) exists for the conductivity of metals (the oscillator-strength sum rule) [21]. In this sum rule, the appearance of the

energy gap of Cooper pairs induces a missing area near $\omega = 0$ in the integrand of the sum rule, hence leading to the $\delta(\omega)$ peak of the supercurrent. The energy gap of Cooper pairs plays two roles, (1) the bosonization of two fermions and (2) the induction of a supercurrent. Such an energy gap does not exist in intrinsic bosons. Rather, the transformation of the fluidity spectrum from the upper-convex to the lower-convex form such as Fig.2 results in a missing area in the integrand, hence leading to $A\delta(\omega)$ of a superfluid flow. Since this transformation is induced by the statistical gap, it controls the phenomenon behind the scenes.

Behind this difference, there is an important difference in the nature of the transition. The phenomenon occurring in fermions in the vicinity of T_c is not gradual growth of the macroscopic coherent wave function, but the abrupt formation of Cooper pairs by the various combinations of two fermions. Once Cooper pairs form, they are already composite bosons with a high density at a low temperature, and they immediately form the superfluid state. Hence, the $\delta(\omega)$ peak and the energy-gap structure of Cooper pairs are not smoothly connected in the excitation spectrum of superconductors.

In contrast, helium 4 atoms at $T \gg T_\lambda$ are intrinsic bosons, although they have not yet formed a macroscopic coherent wave function. As $T \rightarrow T_\lambda$, the coherent wave function gradually grows. Hence, even if it occurs within a very narrow temperature region above T_λ , we can consider the growth process of a superfluid flow as a transformation of the nonequilibrium steady process. In this case, the $\delta(\omega)$ peak and $\sigma_s(\omega)$ at $\omega \neq 0$ are smoothly connected in the spectrum, which reflects the growth process of a superfluid flow.

B. Role of the repulsive interaction

The role of the repulsive interaction in a superfluid flow is an important problem.

(1) In general, the repulsive interaction stabilizes the condensate by preventing the fragmentation of the condensate [30]. If it fragments into two condensates, the exchange energy due to the repulsive interaction makes it costly. Hence, the repulsive interaction is a premise of our thermodynamic consideration, and the size distribution $h(s) = \exp(\beta\mu s)/s$ of the coherent wave function is not an exception.

(2) The mean-field effect U_0 of the repulsive interaction considerably changes the fluidity spectrum as shown in Figs.11 and 12. As shown in Figs.6 and 7, however, $\tilde{A}(T)$ of a superfluid flow does not depend on U_0 at T_λ .

(3) The many-body effect of the repulsive interaction U on a superfluid flow is a difficult problem. To describe its many-body effect, the perturbation expansions of $\chi^L(\mathbf{q}, \omega)$ and $\chi^T(\mathbf{q}, \omega)$ in powers of U are needed. Their structures are different, because the roles of the repulsive interaction in the longitudinal and transverse cases are considerably different.

As a first approximation, we here consider only a chain reaction of the longitudinal excitation from the condensate, and the decay to it. In $\chi_{\mu\nu}(\mathbf{q}, \omega)$ of Eq.(45), we replace $\chi^L(\mathbf{q}, \omega)$ at $\omega > 0$ by a sum of bubble-chain-type diagrams as follows

$$\begin{aligned} \chi^L(\mathbf{q}, \omega) &= -\frac{\hbar^2}{4} \sum_s \left(\frac{sh(s)}{\hbar\omega - \hbar a_l q^2} + \frac{-sh(s)}{\hbar\omega + \hbar a_l q^2} \right) q^2 \\ &\times \left[\sum_{n=0}^{\infty} U^n \left(\frac{sh(s)}{\hbar\omega - \hbar a_l q^2} + \frac{-sh(s)}{\hbar\omega + \hbar a_l q^2} \right)^n \right]. \end{aligned} \quad (66)$$

Substituting this $\chi^L(\mathbf{q}, \omega)$ into $\chi^L(\mathbf{q}, \xi)$ ($-\infty < \xi < \infty$) of Eq.(41), we obtain a new fluidity spectrum in place of Eq.(46),

$$\begin{aligned} \sigma_1(\omega) &= \sigma_{1n}(\omega) + \frac{\hbar}{2\pi} \frac{1}{4\eta_n} a \int dq^2 \sum_s sh(s) \frac{q^2}{\omega} \int_{-\infty}^{\infty} d\xi \\ &\times \frac{1}{\xi - \omega} \left(\frac{1}{\xi - a_l q^2} - \frac{1}{\xi - \epsilon_t(s, q)/\hbar} \right) \\ &+ \frac{\hbar}{2\pi} \frac{1}{4\eta_n} a \int dq^2 \sum_{n=1}^{\infty} \frac{U^n}{\hbar^n} \\ &\times \sum_s [sh(s)]^{n+1} \frac{q^2}{\omega} \int_{-\infty}^{\infty} d\xi \frac{1}{\xi - \omega} \left(\frac{1}{\xi - a_l q^2} \right)^{n+1}. \end{aligned} \quad (67)$$

For the third term, after defining a new variable $x = \xi - a_l q^2$, the Hilbert transformation of $1/x^n$ is performed. Such a formula is obtained by repeating the differentiation of $1/(x + i\epsilon) = 1/x - i\pi\delta(x)$ with respect to x by n times,

$$\frac{1}{\pi} \int_{-\infty}^{\infty} \frac{dx}{x - \omega} \frac{1}{x^n} = -\pi \frac{(-1)^n}{\Gamma(n)} \delta^{(n-1)}(\omega), \quad (68)$$

where $\delta^{(n)}(\omega)$ is the n th derivative of $\delta(\omega)$. Applying this formula to Eq.(67) yields

$$\begin{aligned} \sigma_1(\omega) &= \sigma_{1n}(\omega) + \frac{\pi\hbar}{2} \frac{1}{4\eta_n} a \int dq^2 \\ &\times \sum_s sh(s) \frac{q^2}{\omega} [\delta(\omega - a_l q^2) - \delta(\omega - \epsilon_t(s, q)/\hbar)] \\ &+ \frac{\pi\hbar}{2} \frac{1}{4\eta_n} a \int dq^2 \sum_{n=1}^{\infty} \frac{U^n}{\hbar^n} \\ &\times \sum_s [sh(s)]^{n+1} \frac{q^2}{\omega} \frac{(-1)^{n+1}}{\Gamma(n+1)} \delta^{(n)}(\omega - a_l q^2) \end{aligned} \quad (69)$$

The third term shows that more singular functions $\delta^{(n)}(\omega)$ than $\delta(\omega)$ appear. However, the presence of $(-1)^{n+1}$ means that these functions almost cancel each

other. Hence, it is unclear whether the many-body effect of the repulsive interaction enhances or suppresses the superfluid flow, at least within the bubble-chain approximation. For this reason, we used Eq.(55) in the sum rule.

For rotational superfluidity, the many-body effect of the repulsive interaction U enhances the anomalous rotational behavior of the Bose systems just above T_λ [24] [31]. For translational superfluidity, however, the many-body effect of U does not necessarily enhance the superfluid flow. The anisotropic effective masses m_t and m_l in the flow are created as the many-body effect of the repulsive interaction. If m_t increases in the sum rule [Eq.(64)], the superfluid flow $\tilde{A}(T)$ will be suppressed. For more precise treatment, it is necessary to begin with the dynamical model of a liquid, which still remains as an undeveloped area.

(4) The experiment using a capillary shows that the flow rate of the superfluid flow does not depend on the length L of the capillary, but strongly depends on its diameter. In this work, we focus on the flow velocity along the axis of the capillary. To derive the dependence of the superfluid flow velocity on the diameter, we must extend the formalism to any distance r from the axis, and integrate these results over the distance from zero to the radius d of the capillary.

C. Gradual decrease in viscosity at $T_\lambda < T < 3.7$ K

In this paper, we focus on the abrupt decrease in the kinematic viscosity $\nu(T)$ at T_λ , but the gradual fall of $\nu(T)$ at $T_\lambda < T < 3.7$ K in Fig.1 is not yet explained.

In the simplest two-fluid model, Eq.(55) gives

$$\sigma_1(\omega) = \sigma_{1n}(\omega) + \tilde{A}(T) \frac{\pi}{d^2} \delta(\omega). \quad (70)$$

For comparison with the experiment, we define a frequency-averaged fluidity $\sigma = \int_{-\infty}^{\infty} \sigma(\omega) d\omega$ using this $\sigma_1(\omega)$, obtaining the coefficient of kinematic viscosity $\nu(T) = 1/(4\sigma)$ as

$$\nu(T) = \frac{\nu_n}{1 + \frac{\tilde{A}(T)}{\sigma_{1n}} \frac{\pi}{d^2}}, \quad (71)$$

where $\nu_n (= 1/[4\sigma_{1n}])$ is ν of the normal phase. This formula means that the gradual fall of viscosity at $T_\lambda < T < 3.7$ K is caused by the gradual increase in $\tilde{A}(T)$ in Eq.(71). The gradual fall of $\nu(T)$ already begins at $2.8 \text{ K} < T < 3.7 \text{ K}$, but $\tilde{A}(T)$ is so small that it cannot explain such a large fall of $\nu(T)$.

Historically, this gradual fall has been tacitly attributed to thermal fluctuation, which has not been explicitly distinguished from the well-known anomalies at $|T/T_\lambda - 1| < 10^{-2}$. (The exception was Ref.5, in which the authors pointed out that the fall of η in the range of $T_\lambda < T < 3.7$ K does not come from thermal fluctuations,

but from the gradual change in the particle distribution occurring above T_λ .) If we adhere to the naive analogy to the ideal Bose gas, nothing occurs above T_λ except for the fluctuation. In view of the complex nature of a liquid, however, it is unnatural to assume that the ideal Bose gas picture grasps the specific features of a strongly interacting dense system, even if it is liquid helium 4.

Physically, the interpretation that $\nu(T)$ in the range of $T_\lambda < T < 3.7$ K comes from thermal fluctuation has the following difficulty. The temperature width of 1.5 K between T_λ and 3.7 K is too large for the thermal fluctuation to occur. The temperature width δT of the fluctuation is given by the well-known formula

$$\langle(\delta T)^2\rangle = \frac{k_B T^2}{C_V}, \quad (72)$$

in which C_V is the specific heat of a small fluctuating region [32]. C_V derived from $\delta T = 1.5$ K in Eq.(72) is about 2.8×10^{-23} J/K. As mentioned in Ref.5, if the interpretation on the basis of fluctuation was true, the fluctuating region corresponding to this value of C_V would be as small as one atom diameter. This result implies that the thermodynamic stability of the macroscopic system does not allow such a wide temperature width δT for fluctuation.

The key to understanding this gradual fall of viscosity is the repulsive interaction. The particles with $\mathbf{p} \neq 0$ in the flow are likely to behave similarly to other particles, especially with the particles having $\mathbf{p} = 0$. If the former behave differently from the latter in the flow, the increase in the repulsive interaction energy is unavoidable. Hence, a considerable number of particles show a singular dynamical behavior even at the temperature for which not all particles participate in the BEC in the thermodynamical sense. In such a case, although the BEC transition is a discontinuous change in the thermodynamic properties, it appears to be a continuous one in the dynamical properties. If this picture is true, the kinematical approach will be useful for discussing $\nu(T)$ in the range of $T_\lambda < T < 3.7$ K. The microscopic formulation of the gradual fall of viscosity is a future problem.

Appendix A: Sum rule

From the general principle, it is proved that the fluidity spectrum $\sigma(\omega)$ must satisfy the sum rule [33]. In general, the susceptibility $\chi(\omega)$ is expressed by the response function $\phi(t)$ as

$$\chi(\omega) = \lim_{\epsilon \rightarrow 0} \int_0^\infty \phi(t) \exp(-i\omega t - \epsilon t) dt, \quad (A1)$$

while the relaxation function $\Phi(t)$ is expressed by this $\phi(t)$ as

$$\Phi(t) = \lim_{\epsilon \rightarrow 0} \int_t^\infty \phi(t') \exp(-\epsilon t') dt'. \quad (A2)$$

The fluidity spectrum $\sigma(\omega)$ is expressed by this $\Phi(t)$ as

$$\sigma(\omega) = \int_0^\infty \Phi(t) \exp(-i\omega t) dt. \quad (A3)$$

Hence, we obtain the sum rule

$$\int_{-\infty}^\infty \sigma(\omega) d\omega = \pi \Phi(0), \quad (A4)$$

in which the right-hand side depends only on the basic parameters of the system. Such parameters determine the initial condition of relaxation at $t = 0$, an example of which is $\pi \rho L/m$ in Eq.(14).

Appendix B: Chemical potential of the ideal Bose gas just above the transition temperature

From the equation of states for N/V in the ideal Bose, we obtain

$$1 = \frac{1}{N} \frac{1}{e^{-\beta\mu} - 1} + \frac{V}{N} \frac{g_{3/2}(e^{\beta\mu})}{\lambda^3}, \quad (B1)$$

where $g_{3/2}(z) = \sum_n^\infty z^{-n}/n^{3/2}$. The critical value v_c at $T = T_0$ is given by

$$v_c = \frac{\lambda_0^3}{g_{3/2}(1)}. \quad (B2)$$

Just above T_0 , V/N on the right-hand side of Eq.(B1) can be approximated by Eq.(B2) as

$$1 = \frac{1}{N} \frac{1}{e^{-\beta\mu} - 1} + \left(\frac{\lambda_0}{\lambda}\right)^3 \frac{g_{3/2}(e^{\beta\mu})}{g_{3/2}(1)}. \quad (B3)$$

We are interested in $\mu(T)$ just above T_0 , which is implicitly included in Eq.(B3). For this purpose, the following expansion is useful [34]

$$g_{3/2}(e^{\beta\mu}) = 2.612 - 2\sqrt{\pi}(\beta\mu)^{0.5} + 1.460\beta\mu - 0.104(\beta\mu)^2 + 0.00425(\beta\mu)^3 - \dots \quad (B4)$$

For $g_{3/2}(e^{\beta\mu})$ in Eq.(B3), we use the first and second terms in this expansion, and obtain Eq.(B3) in the first order of $\sqrt{\beta\mu}$ as

$$1 = \frac{1}{N|\beta\mu|} + \left(\frac{T}{T_0}\right)^{1.5} \left[1 - \frac{2\sqrt{\pi}}{g_{3/2}(1)} \sqrt{|\beta\mu|}\right]. \quad (B5)$$

Defining $|\beta\mu| \equiv x$, we obtain

$$\left(\frac{T}{T_0}\right)^{1.5} \frac{2\sqrt{\pi}}{g_{3/2}(1)} x^{1.5} + \left[1 - \left(\frac{T}{T_0}\right)^{1.5}\right] x = \frac{1}{N}. \quad (B6)$$

For a small $|\beta\mu| > 1/N$, we can neglect $1/N$ on the right-hand side, and obtain

$$x = \left(\frac{g_{3/2}(1)}{2\sqrt{\pi}}\right)^2 \left[\left(\frac{T_0}{T}\right)^{1.5} - 1\right]^2. \quad (B7)$$

Just above T_0 , the right-hand side is expanded in powers of $T - T_0$, hence

$$\mu_0(T) = - \left(\frac{2.612 \times 3}{4\sqrt{\pi}} \right)^2 k_B T_0 \left(\frac{T - T_0}{T_0} \right)^2. \quad (\text{B8})$$

Appendix C: Combinatorial derivation of Eq.(27)

The partition function $Z_0(N)$ of an ideal Bose gas is written in a form reflecting the growth of the coherent wave function in configuration space,

$$Z_0(N) = \frac{1}{N!} \left(\frac{m}{2\pi\beta\hbar^2} \right)^{3N/2} \times \int \sum_{\text{per}} \exp \left[-\frac{m}{2\beta\hbar^2} \sum_i^N (x_i - P x_i)^2 \right] d^N x_i, \quad (\text{C1})$$

where P denotes permutation. To calculate $Z_0(N)$, a geometrical consideration on the distribution of the coherent wave function is needed [19].

(a) Let us consider an elementary unit of the partition function $Z_0(N)$. The s -size coherent wave function appears in the integral of Eq.(C1) as

$$\int \exp \left[-\frac{m}{2\beta\hbar^2} (x_{12}^2 + \dots + x_{s1}^2) \right] d^s x_i \equiv L_s, \quad (\text{C2})$$

where $x_{ij}^2 = (x_i - x_j)^2$. If the last term x_{s1}^2 in the exponent is replaced by x_{s0}^2 , it becomes an open graph, and L_s becomes a function of $x_1 - x_0 (\equiv x_{10})$ as

$$\widehat{L}_s(x_{10}) = \int \exp \left[-\frac{m}{2\beta\hbar^2} (x_{12}^2 + \dots + x_{s0}^2) \right] d^{s-1} x_i. \quad (\text{C3})$$

This $\widehat{L}_s(x_{10})$ is related to L_s as $L_s = \widehat{L}_s(x_{10} = 0)$, and is simply obtained by $(s-1)$ convolutions of $\exp(-mx_i^2/2\beta\hbar^2)$ with the initial one $\exp(-mx_1^2/2\beta\hbar^2)$. To obtain $\widehat{L}_s(x_{10})$, the convolution theorem states that one must calculate a three-dimensional Fourier-transformed function $\Gamma(p)$ for each x ,

$$\Gamma(p) = \int \exp \left[-\frac{mx^2}{2\beta\hbar^2} \right] \exp(ip \cdot x) d^3 x = \lambda'^3 \exp \left(-\frac{\lambda'^2 p^2}{2} \right), \quad (\text{C4})$$

where $\lambda' = \lambda_t / \sqrt{2\pi}$ (λ_t is the thermal wavelength). Moreover, one must obtain an inverse-Fourier-transformed function of $\Gamma(p)^s$ with respect to x_{10} as

$$\widehat{L}_s(x_{10}) = \frac{V}{(\sqrt{2\pi})^3} \int (\sqrt{2\pi})^{3(s-1)} \Gamma(p)^s e^{-ipx_{10}} 4\pi p^2 dp, \quad (\text{C5})$$

where V comes from the translation of the closed graph. Since $L_s = \widehat{L}_s(x_{10} = 0)$, one has

$$L_s = V \int (\sqrt{2\pi})^{3s} \Gamma(p)^s \frac{4\pi p^2 dp}{(2\pi)^3}. \quad (\text{C6})$$

This integral, after using

$$\int_0^\infty \exp(-ap^2) p^2 dp = \frac{1}{8} \sqrt{\pi/a^3}, \quad (\text{C7})$$

for $\Gamma(p)$ in Eq.(C4), yields

$$L_s = V \left(\lambda^{3s} + \frac{1}{2} \lambda^{3(s-1)} \frac{V}{s^{3/2}} \right), \quad (\text{C8})$$

where the first term λ^{3s} is obtained by extracting $\Gamma(p = 0)$ from Eq.(C6).

(b) Let us consider a situation in which elementary closed graphs of size s appear ξ_s times in $Z_0(N)$, with a distribution $\{\xi_1, \xi_2, \dots, \xi_s, \dots\}$ being subject to $N = \sum_s s \xi_s$. Consider the number of all possible configurations represented by $\{\xi_1, \dots, \xi_s, \dots\}$, and denote it with $B(\xi_1, \dots, \xi_s, \dots)$. One can rewrite Eq.(C1) as

$$Z_0(N) = \frac{1}{N!} \left(\frac{m}{2\pi\beta\hbar^2} \right)^{3N/2} \times \sum_{\{\xi_s\}} B(\xi_1, \dots, \xi_s, \dots) L_1^{\xi_1} \dots L_s^{\xi_s} \dots \quad (\text{C9})$$

$B(\xi_1, \dots, \xi_s, \dots)$ is estimated as follows. Assume N particles in an array. The number of ways of partitioning them into $\{\xi_1, \dots, \xi_s, \dots\}$ is given by $N! / \Pi_s \xi_s!$. An array of s particles corresponds to a closed graph of size s . For the coherent wave function, it does not matter which particle is the initial one in the array (circular permutation). Hence, $N! / \Pi_s \xi_s!$ must be multiplied by a factor $1/s$ for each ξ_s , with the result that

$$B(\xi_1, \dots, \xi_s, \dots) = \frac{N!}{\prod_s \xi_s! s^{\xi_s}}. \quad (\text{C10})$$

With this B used in Eq.(C9), one obtains

$$Z_0(N) = \frac{1}{\lambda^{3N}} \sum_{\{\xi_s\}} \prod_s \frac{1}{\xi_s!} \left(\frac{L_s}{s} \right)^{\xi_s}. \quad (\text{C11})$$

Using this $Z_0(N)$, the grand partition function

$$Z_0(\mu) = \sum_N Z_0(N) e^{\beta\mu N} \quad (\text{C12})$$

is obtained as follows. The summation over N under $\sum_s s \xi_s = N$ changes to a free summation over ξ_s from 0 to ∞ . After substituting $N = \sum_s s \xi_s$ into λ^{3N} in Eq.(C11), and into $e^{\beta\mu N}$ in Eq.(C12), this summation yields the exponential form

$$Z_0(\mu) = \prod_s \exp \left[\frac{L_s}{s} \left(\frac{e^{\beta\mu}}{\lambda^3} \right)^s \right]. \quad (\text{C13})$$

Using Eq.(C8) for L_s in this $Z_0(\mu)$, one obtains Eq.(27).

Appendix D: Spectral analysis of rotational superfluid-flow

The Hamiltonian in a coordinate system rotating with a container is $H - \mathbf{\Omega} \cdot \mathbf{L}$, where \mathbf{L} is the total angular momentum and $\mathbf{\Omega}$ is the applied angular velocity. The perturbation $H_{ex} = -\mathbf{\Omega} \cdot \mathbf{L}$ is cast in the form $-\sum_i (\mathbf{\Omega} \times \mathbf{r}) \cdot \mathbf{p}$, in which $\mathbf{\Omega} \times \mathbf{r} \equiv \mathbf{v}_d(\mathbf{r})$ serves as the external field. Defining a mass-current density $\mathbf{J}(\mathbf{r})$, we express the perturbation H_{ex} as

$$-\mathbf{\Omega} \cdot \mathbf{L} = - \int \mathbf{v}_d(\mathbf{r}) \cdot \mathbf{J}(\mathbf{r}) d^3x. \quad (\text{D1})$$

Because of $\text{div} \mathbf{v}_d(\mathbf{r}) = 0$, $\mathbf{v}_d(\mathbf{r})$ acts as a transverse-vector probe to the excitation of bosons. For the rotation, one must use the transverse susceptibility $\chi^T(q, \omega)$ for $\mathbf{v}_d(\mathbf{r})$ such as $\mathbf{J}(\mathbf{r}) = [\lim_{q \rightarrow 0} \chi^T(q, 0)] \mathbf{v}_d(\mathbf{r})$. Using $\mathbf{\Omega} = (0, 0, \Omega)$ on the left-hand side of Eq.(D1), and using the above $\mathbf{J}(\mathbf{r})$ and $\mathbf{v}_d = \mathbf{\Omega} \times \mathbf{r} = (-\Omega y, \Omega x, 0)$ on its right-hand side, one obtains the angular momentum L_z as

$$L_z = \chi^T(0, 0) \int_V (x^2 + y^2) d^3x \cdot \Omega. \quad (\text{D2})$$

In a normal fluid, the susceptibility satisfies $\chi^T(0, 0) = \chi^L(0, 0)$, and therefore the ordinary use of ρ is justified. The classical moment of inertia is given by

$$I_z^{cl} = mn \int_V (x^2 + y^2) d^3x = \chi^L(0, 0) \int_V (x^2 + y^2) d^3x. \quad (\text{D3})$$

In a superfluid, however, we must go back to Eq.(D2), and write the moment of inertia $I_z = L_z/\Omega$ as

$$I_z = I_z^{cl} \left(1 - \frac{1}{\rho} \lim_{q \rightarrow 0} [\chi^L(q, 0) - \chi^T(q, 0)] \right). \quad (\text{D4})$$

For the dynamic response, the current $\mathbf{J}(\mathbf{r}) = \chi^T(0, 0) \mathbf{v}_d(\mathbf{r})$ is replaced by $\mathbf{J}(\mathbf{r}) = \chi^T(0, 0, \Omega, r) \mathbf{v}_d(\mathbf{r})$, where $r = \sqrt{x^2 + y^2}$ is the distance from the center of rotation. Correspondingly, we define

$$L_z = \int_V \chi^T(0, 0, \Omega, r) r^2 d^3x \cdot \Omega, \quad (\text{D5})$$

and

$$I_z(\Omega) = I_z^{cl} - \lim_{q \rightarrow 0} \int_V [\chi^L(q, 0, \Omega, r) - \chi^T(q, 0, \Omega, r)] r^2 d^3x. \quad (\text{D6})$$

The position-dependent angular velocity is defined as

$$\mathbf{\Omega}_0(\mathbf{r}) = \left(1 - \frac{1}{\rho} \lim_{q \rightarrow 0} [\chi^L(q, 0, \Omega, r) - \chi^T(q, 0, \Omega, r)] \right) \mathbf{\Omega}. \quad (\text{D7})$$

Let us consider the first approximation of the above quantities. We begin with

$$\langle J_\mu(x, t) \rangle = \langle G | S^\dagger \hat{J}_\mu(x, t) S | G \rangle, \quad (\text{D8})$$

where $S = T \exp \left[-i \int_{-\infty}^t dt' \hat{H}_{ex}(\mathbf{r}, t') \right]$. Using $H_{ex}(\mathbf{r}) = -v_d^\mu(\mathbf{r}) J_\mu(\mathbf{r})$, the analytical continuation $t \rightarrow$

$\tau = it$ is performed in the higher-order expansion terms on the right-hand side of Eq.(D8). As the simplest non-linear susceptibility for J_μ , we consider the third-order term $\chi_{\mu, \nu \sigma \tau}^{(3)} v_d^\nu v_d^\sigma v_d^\tau$ with respect to H_{ex} , and extract a correction term to the linear susceptibility $\chi_{\mu\nu}^{(3)}(v_d) \mathbf{v}_d$ from $\chi_{\mu, \nu \sigma \tau}^{(3)} v_d^\nu v_d^\sigma v_d^\tau$ as

$$\begin{aligned} \chi_{\mu\nu}^{(3)}(q, i\omega) &= \beta n_0 |\mathbf{v}_d(\mathbf{r})|^2 \frac{1}{\beta^2} \sum_{n,m} \frac{1}{V^2} \sum_{p, p_1} \left(p + \frac{q}{2} \right)_\mu \\ &\times \left(p_1 + \frac{q}{2} \right)_\nu \left(\frac{p + p_1}{2} \right) \cdot \left(\frac{p + p_1}{2} + q \right) \\ &\times G(i\omega_n + i\omega, p + q) G(i\omega_n, p) \\ &\times G(i\omega_m + i\omega, p_1 + q) G(i\omega_m, p_1), \end{aligned} \quad (\text{D9})$$

where

$$G(i\omega_n, p) = \frac{1}{i\omega_n - \epsilon(p) - \Sigma + \mu}. \quad (\text{D10})$$

As a result, we obtain

$$\hat{\chi}_{\mu\nu}^{(3)}(q, 0, \Omega, r) = -q_\mu q_\nu \frac{1}{V^2} \left(\frac{q^2}{4} \right) |F_\beta(q)|^2 (\Omega r)^2 \beta n_0(T), \quad (\text{D11})$$

where

$$F_\beta(q) = \frac{(\exp(\beta[\Sigma - \mu]) - 1)^{-1} - (\exp(\beta[\epsilon(q) + \Sigma - \mu]) - 1)^{-1}}{\epsilon(q)}, \quad (\text{D12})$$

is a positive monotonically decreasing function of q^2 , which approaches zero as $q^2 \rightarrow \infty$. The infinite sum of the bubble-chain diagrams due to the particle interaction is given by

$$\begin{aligned} \hat{\chi}_{\mu\nu}^{(3)}(q, 0, \Omega, r) &= -\frac{q_\mu q_\nu}{2} \left(\frac{q^2}{2} \right) \frac{1}{V^2} \frac{1}{n^2} \frac{|F_\beta(q)|^2}{[1 - U F_\beta(q)]^2} (\Omega r)^2 \\ &\times \beta n_0(T). \end{aligned} \quad (\text{D13})$$

Hence, we obtain

$$\begin{aligned} \hat{\chi}_{\mu\nu}^{(3)}(q, 0, \Omega, r) &= -\frac{1}{V^2} \left(\frac{2m}{U \beta_{on}} \right)^2 \beta_{on} \frac{1}{n^2} \\ &\times \tanh^2 \left(\frac{\beta_{on} [\mu(T_{on}) - \Sigma]}{2} \right) (\Omega r)^2 \\ &\times n_0(T_{on}) \frac{q_\mu q_\nu}{q^2}. \end{aligned} \quad (\text{D14})$$

Using this result in the next-order term in Eq.(D7), we obtain the Ω -dependent form of the angular velocity of a superfluid in a rotating basket [24] as

$$\mathbf{\Omega}_0(\mathbf{r}) = \left[1 - \frac{\hat{\rho}_s(T)}{\rho} + \frac{1}{c(T)} \left(\frac{\hat{\rho}_s(T)}{\rho} \right)^3 \frac{m(\Omega r)^2}{k_B T} \right] \mathbf{\Omega}. \quad (\text{D15})$$

- [1] P. Kapitza, Nature. **141**, 74 (1938), J. F. Allen and A. D. Meissner, Nature. **141**, 75 (1938).
- [2] L. D. Landau, J.Phys.USSR. **5**, 71 (1941).
- [3] F. London *Superfluid*, (Wiley, New York, 1954) Vol.2.
- [4] Recently, the microscopic image of a liquid has been changing with the progress of experimental and theoretical studies, which is expected to shed new light on this point. (As a review, see K. Trachenko and V. V. Brazhkin, Rep.Prog.Phys. **79**, 016502 (2016).)
- [5] R. Bowers and K. Mendelssohn, Proc. Roy. Soc. Lond. A. **204**, 366 (1950).
- [6] K. N. Zinoveva, Zh.Eksp,Teor.Fiz. **34**, 609 (1958). [Sov.Phys.JETP. **7**, 421 (1958)].
- [7] At $T < T_\lambda$, the temperature dependence of viscosity depends on the type of measurement, although each type gives the same result at $T > T_\lambda$ (*the viscosity paradox*). The shear viscosity of liquid helium 4 measured using an oscillating-disc viscometer, or rotation viscometer, does not drop to zero at $T < T_\lambda$, and shows its characteristic temperature dependence. Such experiments observe the viscous behavior of the normal-fluid component. In contrast, the viscosity of the capillary flow is conceptually the simplest one, because it completely vanishes at $T < T_\lambda$. While the normal-fluid flow is held back with the walls, the superfluid flow can run without any friction. It is this flow rate that the capillary flow experiment observes. [For example, see S.J.Putterman, *Superfluid Hydrodynamics*, (North Holland, Amsterdam, 1974).]
- [8] Bifurcation is a phenomenon in which a simple dynamical process qualitatively changes to a more complex one when an external parameter exceeds a critical value, such as the transition of a laminar flow to a turbulent flow.
- [9] The oscillatory Poiseuille's flow is often used in the experiments on turbulence. The flow velocity v and angular frequency ω in our thought experiment on a superfluid flow are much smaller than those used in the experiments on turbulence.
- [10] Whereas the following argument is applicable to any r , we consider \mathbf{v} along the axis of the capillary ($r = 0$) for simplicity.
- [11] T. Sexl, Z.Phys. **61**, 349 (1930).
- [12] S. Koh, J.Phys.Soc.Jpn. **79**, 054601 (2010). We must correct some conclusions in this reference. (Figure. 2 and Eqs.(11) and (28) of Ref.12 must be replaced by Fig.2 and Eqs. (55) and (71) of the present paper, respectively.)
- [13] R. P. Feynman, Phy.Rev. **94**, 262 (1954), and R. P. Feynman, in *Progress in Low Temp Phys.* vol.1, ed by C.J. Gorter (North-Holland, Amsterdam, 1955) p17.
- [14] For parameters of liquid helium 4, see R. J. Donnelly and C. F. Barenghi, J.Phys.Chem.Ref.Data, **27**, 6, 1217 (1998).
- [15] For example, D.J.Evans and G.Morriss, *Statistical Mechanics of Nonequilibrium Liquids*, 2nd (Cambridge, 2008).
- [16] S. Tomonaga, Prog.Theo.Phys. **13**, 467 (1955), S. Tomonaga, Prog.Theo.Phys. **13**, 482 (1955).
- [17] The increase in kinetic energy caused by the particle exchange in Bose statistics has also been studied in liquid helium 4 with restricted geometries. A path integral calculation shows that when Bose particles are packed into small regions, the permutation originally possible in Bose statistics is prohibited; then, the kinetic energy increases.
- Y. Nakamura and T. Takagi, J.Phys.Soc.Jpn. **77**, 034608 (2008).
- [18] H. Mori, Phy.Rev. **112**, 1829 (1958). J. M. Luttinger, Phy.Rev. **135**.A, 1505 (1964). D.N.Zubarev, *Nonequilibrium Statistical Thermodynamics*, (Springer, 1995).
- [19] R. P. Feynman, Phy.Rev. **91**, 1291 (1953). T. Matsubara, Prog.Theor.Phys. **6**, 714 (1951).
- [20] As a review, see R. Zwanzig, Annu.Rev.Phys.Chem. **16**, 67 (1965).
- [21] Superconductivity was examined using an indirect method and sum rule in M. Tinkham and R. A. Ferrell, Phy.Rev. **2**, 331 (1959). [As a text, see M. Tinkham, *Introduction to Superconductivity*, (McGraw-Hill, 1996, 2nd).] The essential feature of the indirect method is that the external force is taken to be transverse. Hence, the electric field $E(t)$ is represented by a vector potential $A(t)$ as $E(t) = -(1/c)\partial A/\partial t$. In the present paper, we reinterpret $E(t)$ and $A(t)$ as pressure $P(t)$ and the fictitious momentum-like field $Q(t)$ in Eq.(33), respectively, which is an analogue of $-(1/c)\partial A/\partial t = E(t)$.
- [22] M. R. Schafroth, Phy.Rev. **100**, 463 (1955).
- [23] As a review, see P. Nozieres, in *Quantum Fluids* ed. D. E. Brewer (North Holland, Amsterdam, 1966) p1, and G. Baym, in *Mathematical Methods in Solid State and Superfluid Theory* ed. R. C. Clark and G. H. Derrick (Oliver and Boyd, Edinburgh, 1969) p. 121.
- [24] S. Koh, Phy.Rev. B. **74**, 054501 (2006).
- [25] $h(s)$ is a quantity per unit volume as in Eq.(28).
- [26] The propagation of transverse oscillations in a liquid is strongly damped, but the second term in the bracket of Eq.(45) represents the transverse one-particle excitations from the condensate, being a phenomenon before the damping.
- [27] The capillary method is not suitable for the precise measurement of $\nu(T)$, which is normally performed by the oscillating-disc viscometer or the rotation viscometer. In contrast to the $\nu(T)$ by a capillary, however, the $\nu(T)$ by the viscometer does not show an abrupt drop, but a continuous fall. The range of $2.17K < T < 2.18K$ is the region in which such a continuous $\nu(T)$ shows a steepest fall [14]. We cannot more precisely determine the temperature at which $\nu(T)$ abruptly drops in the capillary experiment.
- [28] J. S. Langer and M. E. Fisher, Phy.Rev.Lett. **19**, 560 (1967).
- [29] In response to an external force, a liquid behaves similarly to a solid for a short time, and therefore we can assume the modulus of rigidity G of a liquid during this interval as that in a solid. J. C. Maxwell, Phil.Trans.Roy.Soc. **157**, 49 (1867) in *The scientific papers of J.C.Maxwell*, ed. W.D. Niven (Dover, New York, 2003) vol.2. 26. (See Ref.4).
- [30] P. Nozieres, in *Bose-Einstein Condensation* (ed. A. Griffin, D. W. Snoke and S. Stringari, (Cambridge, 1995).
- [31] S. Koh, Phy.Rev. B. **68**, 144502 (2003).
- [32] For example, L. D. Landau and E. M. Lifshitz, *Statistical Physics*, (Elsevier, 1980) Part 1, 3rd ed.
- [33] R. Kubo, J.Phys.Soc.Jpn. **12**, 570 (1957).
- [34] J. E. Robinson, Phy.Rev. **83**, 678 (1951).